nature communications

Article

https://doi.org/10.1038/s41467-025-58017-9

A tunable and versatile chemogenetic near-infrared fluorescent reporter

Received: 11 April 2024

Accepted: 10 March 2025

Published online: 16 March 2025

Check for updates

Lina El Hajji[1,2], Benjamin Bunel[3], Octave Joliot[4], Chenge Li[1], Alison G. Tebo[1,5], Christine Rampon[1,6], Michel Volovitch[1], Evelyne Fischer[3], Nicolas Pietrancosta[1,7], Franck Perez[4], Xavier Morin[3], Sophie Vriz[1,6] & Arnaud Gautier[1,2,8]

Near-infrared (NIR) fluorescent reporters open interesting perspectives for multiplexed imaging with higher contrast and depth using less toxic light. Here, we propose nirFAST, a small (14 kDa) chemogenetic NIR fluorescent reporter, displaying higher cellular brightness compared to top-performing NIR fluorescent proteins. nirFAST binds and stabilizes the fluorescent state of synthetic cell permeant fluorogenic chromophores (so-called fluorogens), otherwise dark when free. nirFAST displays tunable NIR, far-red or red emission through change of fluorogen. nirFAST allows imaging and spectral multiplexing in live cultured mammalian cells, chicken embryo tissues and zebrafish larvae. Its suitability for stimulated emission depletion nanoscopy enabled protein imaging with subdiffraction resolution in live cells. nirFAST enabled the design of a two-color cell cycle indicator for monitoring the different phases of the cell cycle. Finally, bisection of nirFAST allowed the design of a chemically induced dimerization technology with NIR fluorescence readout, enabling the control and visualization of protein proximity.

Far-red (FR) and near-infrared (NIR) fluorescent proteins (FPs) have opened new possibilities for imaging biological processes in living cells and organisms[1–4]. Spectrally orthogonal to visible fluorescent proteins, biosensors, and optogenetic tools, FR and NIR FPs provide additional colors for highly multiplexed experiments[5,6]. In addition, autofluorescence of most tissues is low in the FR/NIR region, facilitating high-contrast imaging. Finally, FR and NIR fluorescence imaging in living systems is facilitated because light above 600 nm is less toxic for cells and penetrates better into biological tissues.

FR/NIR FPs were engineered from bacterial phytochromes, protein photoreceptors that incorporate covalently the endogenous chromophore biliverdin[3]. Highly fluorogenic, biliverdin only fluoresces when embedded in FR/NIR FPs. The apparent brightness of FR/NIR FPs in cells depends, however, on the availability of biliverdin and its efficacy of incorporation. Efficient incorporation of biliverdin remains a key challenge in the field as biliverdin concentration can vary in cells, and as the kinetics of incorporation is rather slow. A recent comprehensive quantitative study identified emiRFP670, miRFP680, miRFP713, and miRFP720 as the top-performing monomeric FR/NIR FPs in cultured mammalian cells[7]. NIR FPs have largely benefitted from protein engineering efforts, aiming at reducing their size (usually around 35 kDa) to reduce the risk of dysfunctional fusions[4,8], and at enhancing their cellular brightness through improvement of the efficacy of incorporation of biliverdin.

Here, we used a chemogenetic approach to engineer a small tunable NIR fluorescent reporter with quasi-instantaneous fluorescence that can be used as an alternative to biliverdin-based FR/NIR FPs. Dubbed nirFAST (near-infrared fluorescence-activating and

[1]Sorbonne Université, École Normale Supérieure, Université PSL, CNRS, Chimie Physique et Chimie du Vivant (CPCV), 75005 Paris, France. [2]Institut Curie, INSERM, CNRS, Chemical Biology of Cancer (CBC), 75005 Paris, France. [3]Institut de Biologie de l'ENS (IBENS), École Normale Supérieure, CNRS, INSERM, Université PSL, 75005 Paris, France. [4]Institut Curie, Université PSL, CNRS UMR144, Paris, France. [5]Howard Hughes Medical Institute – Janelia Research Campus, Ashburn, VA, USA. [6]Université Paris Cité, 75006 Paris, France. [7]Neuroscience Paris Seine-Institut de Biologie Paris Seine (NPS-IBPS) INSERM, CNRS, Sorbonne Université, Paris, France. [8]Institut Universitaire de France, Paris, France. e-mail: arnaud.gautier@sorbonne-universite.fr

https://doi.org/10.1038/s41467-025-58017-9

absorption-shifting tag), this chemogenetic reporter is composed of a small protein of 14 kDa that efficiently and rapidly assembles with the synthetic fluorogenic chromophore 4-hydroxy-3,5-dimethoxyphenylallylidene rhodanine (HPAR-3,5DOM) to form a fluorescent semi-synthetic assembly with emission maximum at 715 nm when excited with red light (Fig. 1a–e). When free at physiological pH, HPAR-3,5DOM is protonated and absorbs violet-blue light, and is almost non-fluorescent because of ultra-fast non-radiative decay (Fig. 1d). Directed evolution and rational design allowed the engineering of a protein cavity that stabilizes the chromophore in its red-light absorbing deprotonated state, and enables it to adopt an emissive conformation, leading to NIR fluorescence upon red light excitation. In this system, deprotonation increases the electron donation of the phenol moiety leading to red-shifted absorption and emission, while immobilization of the chromophore in a planar conformation slows down non-radiative de-excitation, leading to high fluorescence activation. This

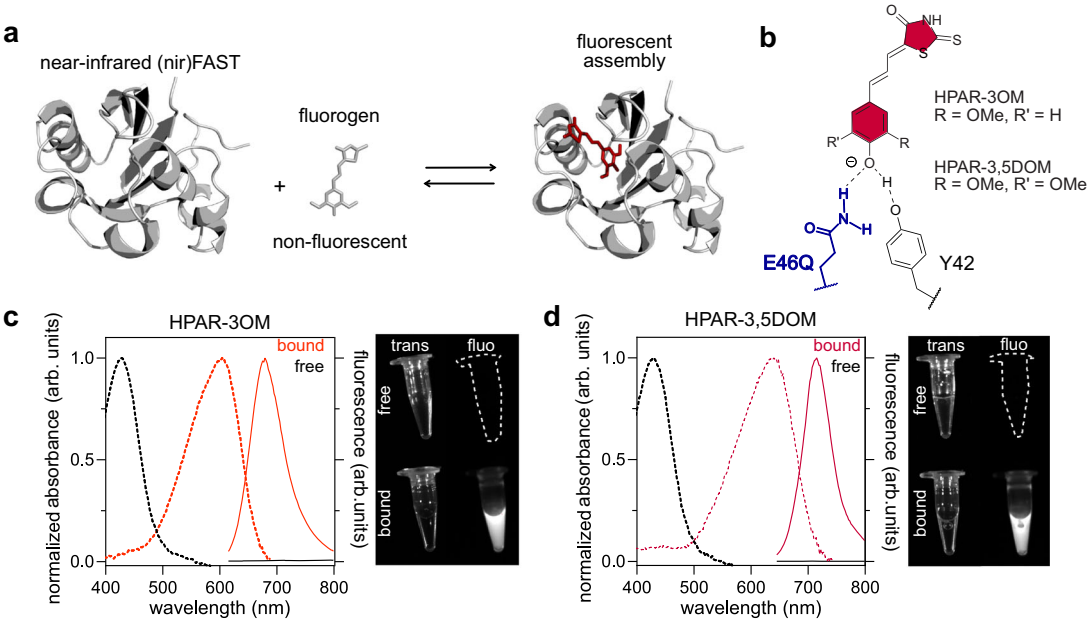

e	K_D (μM)	λ_{abs} (nm)	$FWHM_{abs}$ (nm)	ε ($mM^{-1}.cm^{-1}$)	λ_{em} (nm)	$FWHM_{em}$ (nm)	FQY (%)
nirFAST680	0.055	604	106	52	680	68	20
nirFAST715	0.036	636	118	41	715	58	6.9

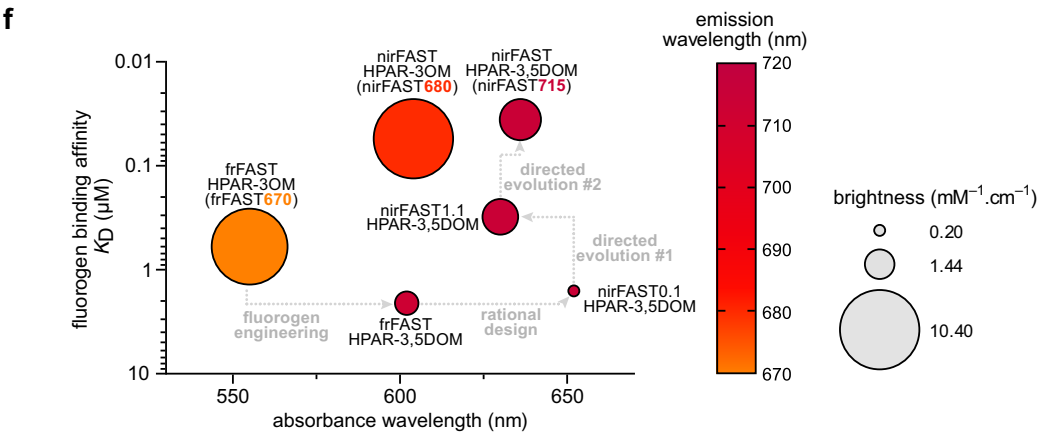

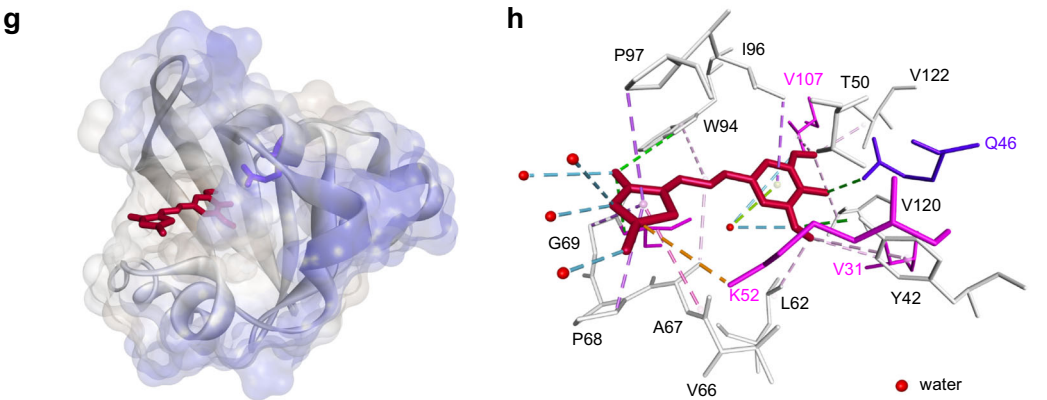

Fig. 1 | nirFAST, a versatile and tunable near-infrared fluorescent chemogenetic reporter. a Principle of nirFAST. **b** Structure of the anionic state of HPAR-3OM and HPAR-3,5DOM in interaction with residues Y42 and Q46. **c** Absorption (dashed line, left axis) and emission (solid line, right axis) spectra of HPAR-3OM free (black) or bound (orange) to nirFAST. Spectra were recorded in pH 7.4 PBS at 25 °C. The image on the right shows the fluorescence of solutions of HPAR-3OM free or bound to nirFAST under illumination with far-red light. **d** Absorption (dashed line) and emission (solid line) spectra of HPAR-3,5DOM free (black) or bound (dark red) to nirFAST. Spectra were recorded in pH 7.4 PBS at 25 °C. The image on the right shows the fluorescence of solutions of HPAR-3,5DOM free or bound to nirFAST under illumination with far-red light. **e** Properties of nirFAST with HPAR-3OM (nirFAST680) and with HPAR-3,5DOM (nirFAST715) in PBS pH 7.4. K_D thermodynamic dissociation constant, λ_{abs} wavelength of maximal absorption, $FWHM_{abs}$ full width at half-maximal absorption, ε molar absorptivity at λ_{abs}, λ_{em} wavelength of maximal emission, $FWHM_{em}$ full width at half-maximal emission, FQY fluorescence quantum yield. **f** Engineering of nirFAST from frFAST670: the thermodynamic dissociation constant K_D, absorption wavelength, emission wavelength, and brightness of the main engineering intermediates are indicated. **g**, **h** Structural model of nirFAST715 generated by homology modeling and molecular dynamics using the crystal structure of the *Halorhodospira halophila* Photoactive Yellow Protein (PYP) (PDB: 6P4I). HPAR-3,5DOM is in red, while Gln46 is in blue. **h** Interactions networks involved in HPAR-3,5DOM binding and recognition within nirFAST. Residues introduced during the engineering process are shown in magenta. See also Supplementary Fig. 6 and Supplementary Data for additional details. Source data are provided as a Source Data file.

unique fluorogenic mechanism provides very high contrast even in the presence of an excess chromophore, allowing wash-free imaging in live cells or organisms. nirFAST can also form a fluorescent assembly with 4-hydroxy-3-methoxyphenylallidene rhodanine (HPAR-3OM) that emits bright fluorescence at 680 nm. In this study, we show that nirFAST (with HPAR-3OM or HPAR-3,5DOM) is brighter than the top-performing emiRFP670 and miRFP713 in cultured mammalian cells when excited at 633 nm, and can be an efficient NIR fluorescent reporter for multiplexed imaging of proteins in mammalian cells, chicken embryo tissues and zebrafish larvae. Its good brightness and photostability make it a well-suited reporter for advanced imaging techniques such as stimulated emission depletion (STED) super-resolution microscopy. We also demonstrate the potential of nirFAST for the design of cellular sensors. The combination of nirFAST with the chemogenetic reporter pFAST[9] allowed the generation of a green-NIR fluorescent ubiquitination-based cell cycle indicator (FUCCI) for visualizing the progression of the cell cycle in living cells. Finally, we also present the use of nirFAST for the design of a fluorogenic chemically induced dimerization technology enabling to control and visualize protein proximity in live cells.

Results

Pushing the spectral properties to the near-infrared

nirFAST was engineered from the chemogenetic fluorescent reporter far-red (fr)FAST[10] (Fig. 1f), a reporter of the fluorescence-activating and absorption-shifting tag (FAST) family (see Supplementary Fig. 1 for a summarizing family tree)[11]. frFAST binds and stabilizes the anionic fluorescent state of HPAR-3OM. The elongated π-electron conjugation in HPAR-3OM gives a fluorescent assembly, hereafter named frFAST670, with a maximal absorption at λ_{abs} = 555 nm and a maximal emission at λ_{em} = 670 nm (Fig. 1f). Despite its FR fluorescence emission, the use of frFAST670 as FR fluorescent reporter is limited by its low absorption in the red region. To obtain a reporter emitting NIR fluorescence (>700 nm) with high efficiency upon excitation with the 633 or 640 nm lasers classically used in fluorescence microscopy and cytometry, we introduced changes in both the fluorogen and the protein (Fig. 1f). Supplementary Note 1 details the full engineering process. In brief, the use of HPAR-3,5DOM, that bears a second methoxy group in the ortho position of the phenol ring, and the mutation of Glu46, which normally stabilizes the phenolate state of the chromophore in frFAST, into glutamine led to a new fluorescent assembly, named nirFAST0.1:HPAR-3,5DOM, with a 95 nm red-shifted absorbance of the anionic phenolate state, and a 45 nm red-shifted emission with respect to frFAST. The assembly nirFAST0.1:HPAR-3,5DOM displayed an absorbance peak at λ_{abs} = 650 nm and an emission maximum at λ_{em} = 715 nm (Fig. 1f, Supplementary Fig. 2a, and Supplementary Table 1), which were ideal for the engineering of a NIR fluorescent reporter excitable with red light. The presence of two methoxy group in ortho position of the phenol in HPAR-3,5DOM (rather than one in HPAR-3OM) shifts absorption and emission to the red by 50 and 40 nm, respectively. The introduction of glutamine in position 46 rather than a glutamic acid additionally shifts the absorption band of the phenolate to the red by 50 nm, presumably because the reduced hydrogen-bond donating ability of glutamine versus glutamic acid increases the electron-donating ability of the anionic phenolate (see Supplementary Note 1 for detailed explanation). However, the introduced modifications resulted in a significant decrease in brightness. Indeed, in nirFAST0.1:HPAR-3,5DOM, the fluorogen is mainly protonated, as evidenced by the presence of a strong absorption band at 430 nm, characteristic of the protonated phenol state, and a much weaker band at 650 nm, characteristic of the deprotonated phenolate (Supplementary Fig. 2a). Since only the deprotonated chromophore absorbs red light, nirFAST0.1:HPAR-3,5DOM displays a low brightness at 650 nm. In addition to decreasing brightness, the modifications of the fluorogen and the mutation E46Q also resulted in a decrease in fluorogen binding affinity (Supplementary Fig. 2b).

Improvement by directed evolution

To increase molecular brightness and fluorogen binding affinity, we used yeast surface display[12] to evolve a protein variant able to efficiently bind and stabilize only the deprotonated state of HPAR-3,5DOM (see also Supplementary Note 1). We created a combinatorial library of variants, which we expressed at the surface of yeast cells. The yeast-displayed library was screened by fluorescence-activated cell sorting (FACS) using a 640 nm excitation laser to sort variants forming bright NIR fluorescent assemblies with HPAR-3,5DOM. After five rounds of enrichment, we isolated and characterized clones with improved brightness. The best clone was further refined by site-directed mutagenesis (Supplementary Figs. 3, 4, Supplementary Tables 1, 2, and Supplementary Note 1). The improved protein, called nirFAST1.1, efficiently binds HPAR-3,5DOM (K_D = 0.31 μM) and forms an assembly tenfold brighter than nirFAST0.1:HPAR-3,5DOM (Fig. 1f and Supplementary Fig. 2a, b).

HPAR-3,5DOM was, however, still partially protonated when embedded in nirFAST1.1 (Supplementary Fig. 2a), therefore we performed a second round of directed protein evolution to maximize deprotonation of the chromophore and thus enhance molecular brightness (see also Supplementary Note 1). This second round of engineering, further refined by site-directed mutagenesis and an additional screening step in mammalian cells (Supplementary Fig. 5), allowed us to identify nirFAST (with the mutations I31V, D36N, Q41K, N43S, E46Q, D48G, R52K, T70S, K78I, I107V relative to frFAST) (Supplementary Figs. 3, 4 and Supplementary Table 3), a protein able to efficiently bind and fully stabilize the deprotonated state of HPAR-3,5DOM. nirFAST shows a tenfold higher fluorogen binding affinity (K_D = 36 nM) relative to nirFAST1.1, ideal for efficient labeling in cells (Supplementary Fig. 2b). With absorption/emission peaks at λ_{abs} = 636 nm and λ_{em} = 715 nm, a fluorescence quantum yield FQY = 6.9% and a maximal molar absorption coefficient $\varepsilon_{636\ nm}$ = 41,000 $M^{-1}.cm^{-1}$, nirFAST:HPAR-3,5DOM shows great molecular brightness in the NIR window while displaying an optimal absorption

maximum for excitation with common 633 and 640 nm red lasers (Fig. 1d–f and Supplementary Fig. 2). Noteworthily, the absorption spectrum of nirFAST:HPAR-3,5DOM was narrower than those of other variants from the engineering process, due to the introduction of the R52K mutation. Overall, nirFAST binds HPAR-3,5DOM 50-fold tighter than nirFAST0.1, and this optimized complex is over 10-fold brighter when excited at 633 nm (Fig. 1f). In addition, free HPAR-3,5DOM is completely non-fluorescent when exciting with red light making it an ideal fluorogen for labeling applications in live systems. Hereafter, the nirFAST assembly with HPAR-3,5DOM is named nirFAST715 for simplicity (the suffix 715 indicates the wavelength of maximal emission).

Interestingly, nirFAST also binds the far-red fluorogen HPAR-3OM with a binding affinity tenfold higher than frFAST (K_D = 55 nM versus 0.6 μM) (Supplementary Fig. 2b). Compared to frFAST670, nirFAST:HPAR-3OM (hereafter called nirFAST680) displays similar fluorescence quantum yield (FQY = 20 %), but is characterized by a 50 nm red-shifted absorption (λ_{abs} = 604 nm), a 10 nm red-shifted emission (λ_{em} = 680 nm) and a narrower absorption spectrum (Fig. 1c, e, Supplementary Fig. 2a and Supplementary Tables 2, 4), making it overall a better FR fluorescent chemogenetic reporter.

Structural model of nirFAST

Homology modeling using the crystal structure of the evolutionary-related photoactive yellow protein (PYP) from *Halorhodospira halophila* (see family tree in Supplementary Fig. 1) coupled to molecular dynamics allowed the generation of an atomic-resolution model of nirFAST715. Within the assembly with minimal energy, the bound HPAR-3,5DOM adopts a quasi-planar conformation in agreement with enhanced fluorescence quantum yield (Fig. 1g, h, Supplementary Fig. 6a–i, and Supplementary Data). HPAR-3,5DOM is stably bound in its deprotonated phenolate state with the phenolate establishing hydrogen bonds with Gln46 (from the rationally introduced E46Q mutation) and Tyr42 (conserved in PYP and all FAST variants) (Fig. 1h), in agreement with the red shifted absorption and emission wavelengths of nirFAST715. The presence of a structural water molecule within the binding cavity stabilizes also the chromophore in its deprotonated state (Fig. 1h and Supplementary Fig. 6b), very likely by influencing the electrostatic environment of the phenolate and thus the local pK_A of the phenol moiety. The Ser70 (from the mutation T70S) establishes hydrogen bonds with this structural water molecule (Supplementary Fig. 6b), stabilizing the overall assembly. All the newly introduced residues are within the chromophore binding pocket or nearby (Supplementary Fig. 6a) and participate in the shaping of the binding pocket. Noteworthily, in addition to Gln46 (from E46Q mutation) that directly interacts with the phenolate of HPAR-3,5DOM, the mutations I31V and I107V widen the bottom of the binding pocket and create a hydrophobic clamp that interacts with the methyl of the methoxy groups of HPAR-3,5DOM (Fig. 1h and Supplementary Fig. 6c). This allows a deeper positioning of the phenolate into the binding cavity, favouring the stabilization of the phenolate by Gln46. The Lys52 (from R52K mutation) also participates in the binding of the chromophore by directly interacting with the rhodanine head of HPAR-3,5DOM (Fig. 1h). In addition, the mutation R52K enables to reduce the size of the binding pocket by allowing the residues 53 to 58 to adopt an α-helix conformation (Supplementary Fig. 6d).

Characterization with prototypical FAST fluorogens

Systematic testing of nirFAST with hydroxybenzylidene rhodanine (HBR) chromophores commonly used with prototypical FAST[13,14], the parent protein of frFAST and nirFAST, showed that nirFAST was able to bind the fluorogens HMBR, HBR-2,5DM, HBR-3,5DM and HBR-3,5DOM, giving respectively, green, yellow, orange and red fluorescence, with moderate or good affinities (Supplementary Table 5). Two opposite behaviors were, however, observed: nirFAST failed to activate efficiently the fluorescence of HMBR and HBR-2,5DM, while it formed bright assemblies with HBR-3,5DM (FQY = 37%) and HBR-3,5DOM (FQY = 24%). The ability of nirFAST to form a tight and bright assembly with HBR-3,5DOM, hereafter called nirFAST600, opened the great prospect for tunable imaging in the red-NIR region of the spectrum as it is possible to generate red, FR, and NIR fluorescence with a single protein tag (nirFAST) through a simple change of fluorogen (vide infra). On the other hand, the inability of nirFAST to activate the green fluorescence of HMBR opened interesting prospects for two-color imaging, leveraging the spectral orthogonality of nirFAST715 and pFAST:HMBR (hereafter called pFAST540) to simultaneously visualize two distinct biological events (vide infra).

Imaging of nirFAST in cultured mammalian cells

Next, we showed that nirFAST could be an efficient NIR fluorescent reporter in cultured mammalian cells. nirFAST expressed in live mammalian cells and labeled with HPAR-3OM or HPAR-3,5DOM displayed a homogenous fluorescence distribution, in agreement with high intracellular stability (Fig. 2a). Fusions of nirFAST to the nuclear histone H2B, to the microtubule-associated protein MAP4, to cytochrome b5 (Cb5) (for anchoring at the membrane of the endoplasmic reticulum) and to the mitochondrial targeting sequence (mito) from the subunit VIII of human cytochrome C oxidase (for expression in the matrix of mitochondria) were correctly localized when expressed in live HeLa cells (Fig. 2a), showing that nirFAST does not perturb cellular localization. Quantitative fluorescence measurements revealed that labeling of nirFAST after cell fixation was as efficient and as contrasted as in live cells (Fig. 2b, c). Fast timelapse confocal microscopy revealed that labeling with HPAR-3OM and HPAR-3,5DOM was complete within twenty seconds of fluorogen addition (Supplementary Fig. 7 and Supplementary Movie 1). Given the typical timescale for small molecule cell uptake and diffusion, these rapid kinetics suggest that labeling is primarily limited by the rate at which the fluorogens can be taken up and diffused into cells. Combined with the observation that HPAR-3OM and HPAR-3,5DOM are non-toxic for mammalian cells at the dose used for imaging (Supplementary Fig. 8), this set of experiments showed that nirFAST was a well-suited protein tag for the selective and efficient labeling of proteins in cultured mammalian cells.

Multicolor imaging in live cells

NIR fluorescent reporters allow multiplexed imaging through combination with visible fluorescent reporters that are spectrally distinct. Efficient multicolor imaging requires, in particular, efficient discrimination between NIR fluorescent reporters and red fluorescent reporters. We showed that, due to its red excitation and NIR emission, nirFAST715 (λ_{abs} = 636 nm, λ_{em} = 715 nm) can be efficiently separated from the red fluorescent protein mCherry (λ_{abs} = 587 nm, λ_{em} = 610 nm) by spectral discrimination, while maximizing the signal of the two reporters (Supplementary Fig. 9). nirFAST715 was superior to nirFAST680 or frFAST670 that both show fluorescence bleed-through in the mCherry channel.

We also demonstrated the possibility of two-color imaging using spectrally orthogonal nirFAST715 and pFAST540 (λ_{abs} = 481 nm, λ_{em} = 540 nm) (Supplementary Fig. 10). Fluorescence microscopy of HeLa cells expressing nirFAST and pFAST in the nucleus and mitochondria after treatment with 1 μM of HMBR and 10 μM of HPAR-3,5DOM showed green fluorescence only in mitochondria and NIR fluorescence only in the nucleus, demonstrating the selective labeling of pFAST with HMBR and nirFAST with HPAR-3,5DOM.

Finally, we showed that nirFAST715 could be combined with the enhanced cyan fluorescent protein (ECFP) (λ_{abs} = 434 nm, λ_{em} = 477 nm), pFAST540, and mCherry for achieving multicolor

https://doi.org/10.1038/s41467-025-58017-9

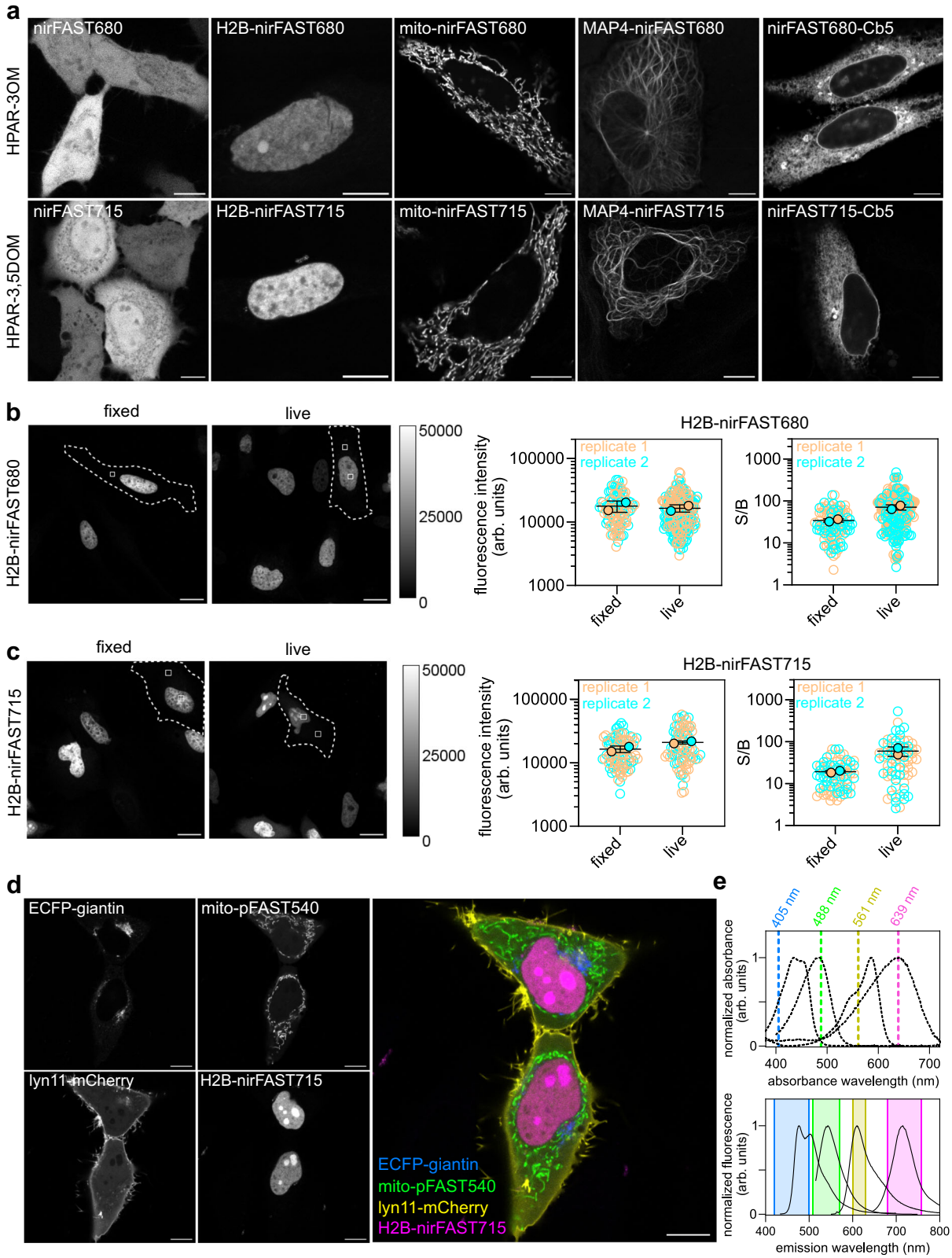

imaging of four cellular targets in live cells. We selectively visualize ECFP localized at the Golgi apparatus through fusion with giantin, the mitochondria-localized mito-pFAST (labeled with HMBR), the inner plasma membrane-anchored lyn11-mCherry and the nuclear H2B-nirFAST (labeled with HPAR-3,5DOM) in HeLa cells using four different excitation lines (405, 488, 561, and 639 nm respectively) and four detection windows (Fig. 2d, e), demonstrating that nirFAST715 could be combined with visible fluorescent reporters for spectral multiplexed imaging of up to four biological targets.

Comparison with top-performing NIR FPs in cultured mammalian cells

Next, we compared nirFAST680 and nirFAST715 with emiRFP670 and miRFP713, two of the top-performing NIR FPs in cultured mammalian

Fig. 2 | Selective imaging of nirFAST in various localizations in mammalian cells. a Live HeLa cells expressing nirFAST-P2A-EGFP or nirFAST fused to: histone H2B, mito (mitochondrial targeting motif), microtubule-associated protein (MAP) 4 and cytochrome b5 (Cb5) for endoplasmic reticulum membrane targeting, and labeled with 10 μM of HPAR-3OM (top row) (to assemble nirFAST680) or HPAR-3,5DOM (bottom row) (to assemble nirFAST715). Scale bars, 10 μm. Representative confocal micrographs from three independent experiments ($n > 13$ cells). **b**, **c** Labeling of H2B-nirFAST in live and fixed cells. Nuclear fluorescence intensity and comparison of signal (nucleus) to background (cytosol) ratio (S/B) in live and fixed cells incubated with 10 μM of HPAR-3OM (to assemble nirFAST680) (**b**) or HPAR-3,5DOM (to assemble nirFAST715) (**c**), and imaged with identical microscope settings. On the graphs, each cell is color-coded according to the biological replicate it came from. The solid circles correspond to the mean of each biological replicate. The black line represents the mean ± SD of the two biological replicates. For nuclear fluorescence evaluation, 103 (respectively 93) fixed cells and 220 (respectively 83) live cells from two independent experiments were used for HPAR-3OM (respectively HPAR−3,5DOM). For S/B evaluation, 103 (respectively 79) fixed cells and 189 (respectively 76) live cells from two experiments were used for HPAR-3OM (respectively HPAR−3,5DOM) analysis. Scale bars, 20 μm. **d** Live HeLa cells co-expressing ECFP fused to giantin, pFAST fused to mitochondria targeting sequence (mito), mCherry fused to lyn11 (inner membrane-targeting motif) and nirFAST fused to H2B. Cells were labeled with 1 μM HMBR to assemble pFAST540 and 10 μM HPAR-3,5DOM to assemble nirFAST715. Representative confocal micrographs from two independent experiments ($n = 22$ cells). Scale bars, 10 μm. **e** Imaging settings and spectral properties of the reporters used in (**d**). Absorption (dashed lines) and emission spectra (solid lines) of ECFP, pFAST540, Cherry, and nirFAST715 are shown. The graph shows the excitation wavelengths and the spectral windows used for imaging. See Supplementary Table 8 for detailed imaging settings. Source data are provided as a Source Data file.

cells (Fig. 3). The two NIR FPs are characterized by fluorescence quantum yields comparable or lower than those of nirFAST680 and nirFAST715, however their molecular brightness in vitro is higher because of higher molar absorption coefficients. emiRFP670 absorbs maximally at 642 nm (with a molar absorption coefficient of 87,400 $M^{-1}.cm^{-1}$) and emits maximally at 670 nm (with a FQY of 14%), while miRFP713 absorbs maximally at 690 nm (with a molar absorption coefficient of 99,000 $M^{-1}.cm^{-1}$) and emits maximally at 713 nm (with a FQY of 7%) (Fig. 3e and Supplementary Table 6)[6]. In cells, the brightness of NIR FPs depends, however, on the intracellular concentration of biliverdin and its efficacy of incorporation. We thus compared the cellular brightness of emiRFP670 and miRFP713 to that of nirFAST680 and nirFAST715. The four proteins were co-expressed stoichiometrically with the green fluorescent protein EGFP using a polycistronic expression cassette containing a viral P2A sequence for ribosomal skipping during translation, allowing us to normalize the NIR fluorescent signal by the protein expression level using the EGFP signal. In HeLa cells, nirFAST680 was 2.5-fold brighter than emiRFP670 when exciting at 633 nm, although absorption at this wavelength is optimal for emiRFP670 and suboptimal for nirFAST680 (Fig. 3a, b, e). Similarly, nirFAST715 was 1.4-fold and 2-fold brighter than emiRFP670 and miRFP713, respectively, when exciting at 633 nm (Fig. 3c–e). Photostability studies in cells showed furthermore that nirFAST680 and nirFAST715 displayed photostability comparable to that of emiRFP670 (Supplementary Fig. 11). The possibility to exchange bleached chromophores with new ones might explain the high photostability, as previously reported for other non-covalent systems[15–17]. Overall, this set of experiments showed that nirFAST was an attractive alternative to NIR FPs for efficient protein imaging in cultured mammalian cells.

Subdiffraction imaging of nirFAST fusions with stimulated emission depletion nanoscopy

Super-resolution microscopy techniques such as stimulated emission depletion (STED) microscopy allow for imaging with spatial resolution beyond the diffraction limit. In STED, super-resolution is achieved by shining a depletion doughnut-shaped laser beam right after excitation[18]. This depletion laser beam switches off fluorophores in the doughnut region through stimulated emission, leaving only the fluorophores at the center in an emissive state. STED requires bright and photostable fluorophores to achieve improved resolution. As nirFAST efficiently formed a bright assembly (nirFAST600) with HBR-3,5DOM (Supplementary Fig. 12), a chromophore which previously allowed STED nanoscopy of pFAST-tagged proteins using a green excitation laser and a 775 nm depletion laser[9], we first demonstrated the STED compatibility of nirFAST using this chromophore. STED microscopy of microtubule-associated MAP4-nirFAST in HeLa cells treated with HBR-3,5DOM allowed us to demonstrate that nirFAST600 was an efficient STED label for the visualization of fine cellular structures in live cells (Fig. 4a), with improved resolution in comparison with regular confocal microscopy (Fig. 4b). Using a parameter-free image resolution estimation method based on image partial phase autocorrelation[19], the resolution enhancement over confocal microscopy was estimated to be 1.6-fold (Fig. 4c).

Although FR and NIR light are less toxic and more compatible with biological imaging, achieving high resolution with FR and NIR reporters is more challenging because of the wavelength-dependence of spatial resolution. In the context of STED, the use of FR and NIR reporters can also be hindered by their possible re-excitation by the 775 nm depletion laser. In this context, we reasoned that nirFAST680 should be well suited for STED nanoscopy because of its remarkably good photostability, brightness, and spectral properties. With a 604 nm excitation peak, nirFAST680 is less prone to re-excitation by the 775 nm depletion beam compared to other NIR reporters with more red-shifted absorption, which should thus increase resolution. In addition, nirFAST680 is efficiently excited at 640 nm, a more favorable wavelength for imaging at high power in living cells. Accordingly, we successfully imaged fine microtubule structures labeled with MAP4-nirFAST680 in live HeLa cells using STED nanoscopy (Fig. 4d), achieving a 1.6-fold resolution enhancement over confocal microscopy (Fig. 4e, f). Overall, this set of experiments showed that nirFAST600 and nirFAST680 were performant STED probes for subdiffraction imaging in live cells.

Imaging of nirFAST in chicken embryo tissues

Next, we investigated the suitability of nirFAST for protein labeling in multicellular organisms using chicken embryo tissues as model. We expressed nirFAST and frFAST in each side of the neural tube (using a sequential in ovo bilateral electroporation strategy) for direct comparison of the two proteins within the very same sample. After dissection of the neural tube, the sample was cultured in an open-book configuration, and labeled with either HPAR-3OM or HPAR-3,5DOM. Simultaneous imaging showed that, with HPAR-3OM, labeling was achieved earlier than 30 min following fluorogen addition with robust NIR signal detected for both frFAST and nirFAST (Fig. 5a, b), confirming efficient permeation of the fluorogen across cell membranes. Fluorescence appears earlier for nirFAST, in agreement with a more efficient binding of HPAR-3OM. Labeling with HPAR-3,5DOM showed high labeling efficiency of nirFAST but poor signal for frFAST (Fig. 5c), in agreement with their relative properties with this fluorogen (Supplementary Table 1). Comparison of the in-tissue brightness of nirFAST715 and emiRFP670 using the same protocol (Fig. 5d) showed that the two proteins displayed comparable fluorescence in chicken embryo tissues, in agreement with the behavior observed in live cultured mammalian cells.

Next, we performed multicolor imaging in chicken embryo tissues. We simultaneously followed the dynamics of nuclear H2B-pFAST540, membrane-anchored mCherry, and mitochondria-localized nirFAST715 during cell division in the neural tube by en-

https://doi.org/10.1038/s41467-025-58017-9

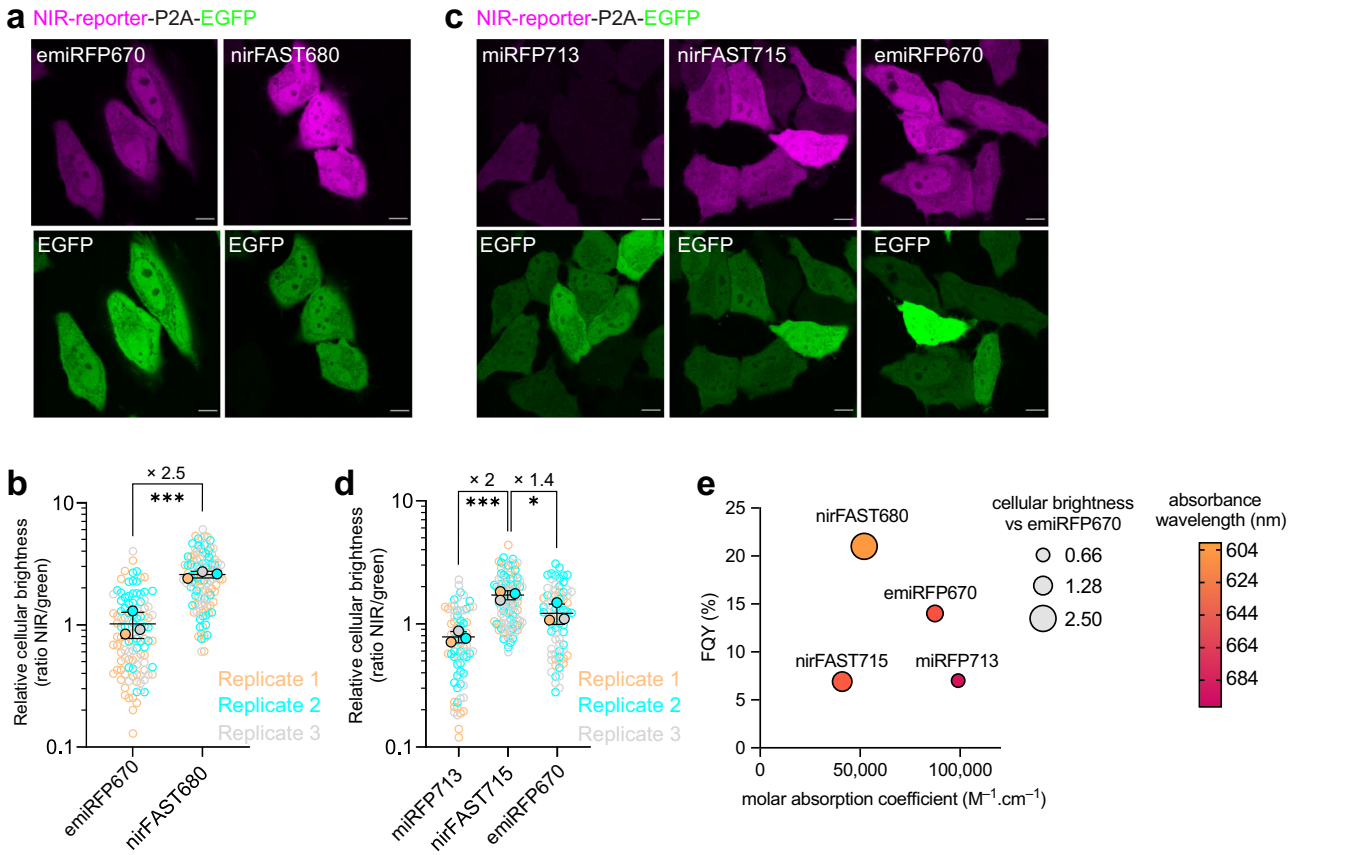

Fig. 3 | Comparison of nirFAST with emiRFP670 and miRFP713. a Hela cells expressing nirFAST-P2A-EGFP (labeled with 10 μM HPAR-3OM to assemble nirFAST680) and emiRFP670-P2A-EGFP. Scale bars, 10 μm. Representative confocal micrographs of $n > 100$ cells from three independent experiments. **b** Relative cellular brightness of nirFAST680 and emiRFP670 computed by normalizing the fluorescence of the NIR reporters with the fluorescence of the stoichiometrically expressed EGFP (ratio NIR/green). Each cell is color-coded according to the biological replicate it came from. The solid circles correspond to the mean of each biological replicate. The black line represents the mean ± SD of the three biological replicates. $n = 115$ (respectively $n = 108$) live cells from three independent experiments were used for nirFAST680 (respectively emiRFP670). An unpaired two-tailed *t*-test assuming equal variance was used to compare the two distributions (***$P = 0.0008$). **c** Hela cells expressing miRFP713-P2A-EGFP, nirFAST-P2A-EGFP (labeled with 10 μM HPAR−3,5DOM to assemble nirFAST715) and emiRFP670-P2A-EGFP. Scale bars, 10 μm. Representative confocal micrographs of n > 70 cells from three independent experiments. **d** Relative cellular brightness of miRFP713, nirFAST715, and emiRFP670 computed by normalizing the fluorescence of the NIR reporters with the fluorescence of the stoichiometrically expressed EGFP (ratio NIR/green). Each cell is color-coded according to the biological replicate it came from. The solid circles correspond to the mean of each biological replicate. The black line represents the mean ± SD of the three biological replicates. n = 106 (respectively $n = 78$ and $n = 74$) live cells from three independent experiments were used for nirFAST715 (respectively miRFP713 and emiRFP670). An unpaired two-tailed *t*-test assuming equal variance was used to compare miRFP713 and nirFAST715 distributions (***$P = 0.0006$, *$P = 0.0340$). **a**–**d** For all these experiments, identical microscope settings were used for enabling side-by-side comparison. **e** Photophysical properties of emiRFP670[6], nirFAST680, miRFP713[6], and nirFAST715. FQY of these reporters are plotted against their molar absorption coefficient. Each data point size is scaled to the cellular fluorescence brightness of the corresponding fluorescent reporter, and the color is indicative of the absorption wavelength. See Supplementary Table 8 for detailed imaging settings. Source data are provided as a Source Data file.

face timelapse imaging of the neuroepithelium (Fig. 5e and Supplementary Movie 2). Labeling of mitochondria with nirFAST715 allowed us to efficiently follow their dynamics during cytokinesis: in metaphase, mitochondria were distributed in the cytoplasm around the metaphase plate; moving to anaphase, mitochondria were recruited at the cell equator at the site of the cleavage furrow and depleted at the cell poles, allowing accurate inheritance of mitochondria between the two daughter cells.

These experiments demonstrated the high suitability of nirFAST for imaging biological processes in complex tissues and highlighted the interest of reporters with NIR-shifted spectral properties for efficient multiplexed imaging.

Imaging of nirFAST in zebrafish embryo

Widely used model for the study of gene function, zebrafish is also an interesting model for cancer-related studies, in particular for investigating cell invasion and metastasis. Injection of cancer cells in zebrafish larvae allows the monitoring of cell growth and proliferation as well as their interaction with their environment by fluorescence imaging[20,21]. In this context, we reasoned that the NIR excitation and emission of nirFAST would make it an interesting alternative to more blue-shifted reporters because of the low autofluorescence of zebrafish tissues in this region of the spectrum. To demonstrate our ability to detect nirFAST-expressing cells in zebrafish larvae, we injected HEK293T cells co-expressing nirFAST and EGFP, near the heart of larvae at 2 dpf (day post fertilization) stage (Fig. 5f, g). Larvae were then imaged two days later by confocal microscopy. After 45 min of treatment with HPAR-3,5DOM, individual cells emitting green and NIR fluorescence were efficiently detected, mainly near the heart. Some cells were also detected from areas close to the inner ear, suggesting cell migration. This experiment showed that nirFAST was well suited for labeling xenografts of mammalian cells injected in zebrafish larvae.

https://doi.org/10.1038/s41467-025-58017-9

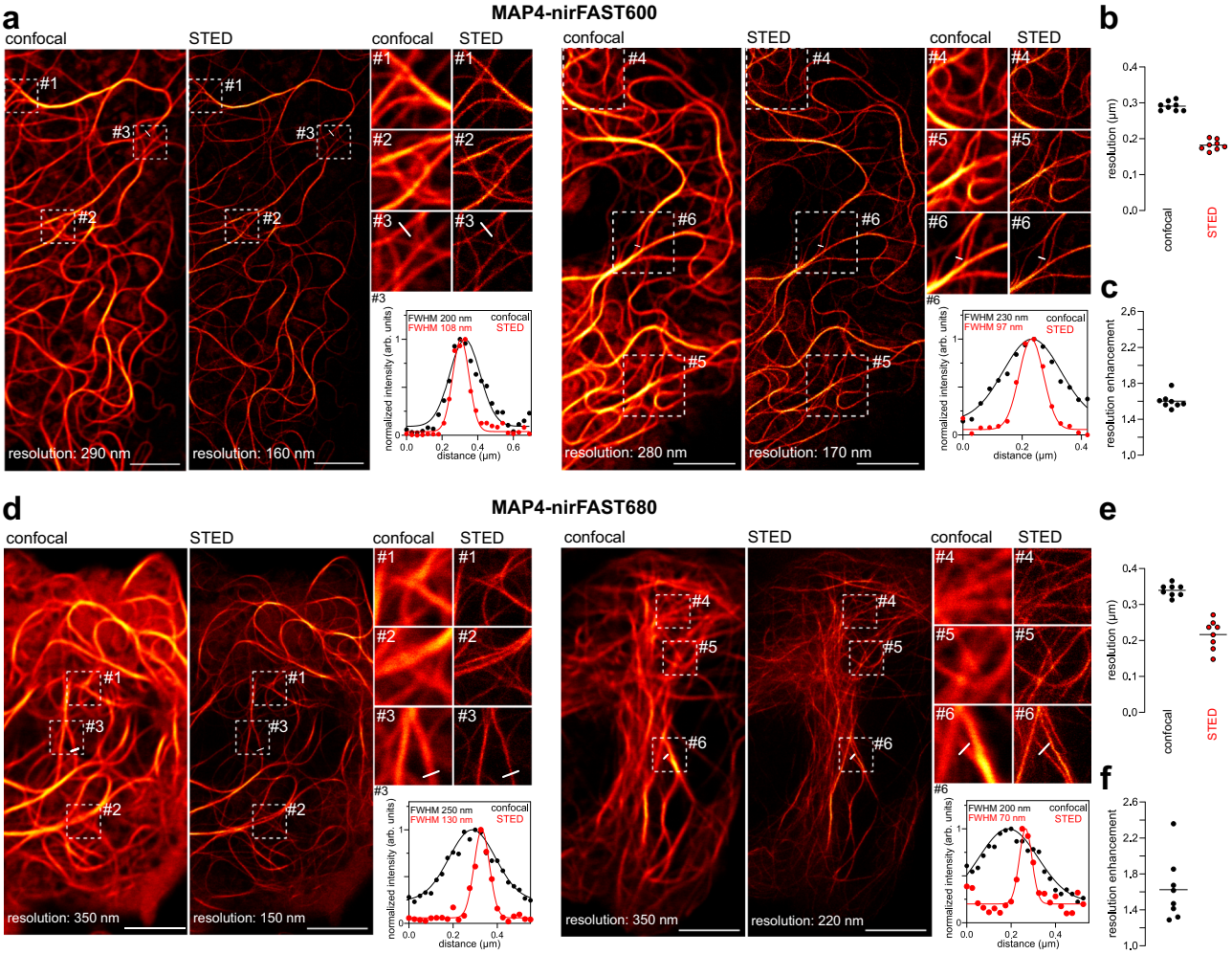

Fig. 4 | STED imaging of nirFAST-tagged proteins in live mammalian cells. Confocal and STED micrographs of two live HeLa cells expressing nirFAST fused to MAP4 and labeled with 10 μM of HBR−3,5DOM (to assemble nirFAST600) (**a**–**c**) or 10 μM of HPAR-3OM to assemble (nirFAST680) (**d**–**f**). For each cell, three regions of interest were selected for close-up comparison between confocal and STED. Line profile across microtubule filaments from one close-up was used to compare the gain in resolution between confocal and STED. Graph shows raw data of line profile from confocal and STED images (points), in addition to the corresponding Gaussian fit (line). Micrographs are representative of $n = 8$ cells from two independent experiments for HBR-3,5DOM (**a**) and HPAR-3OM (**d**). Scale bars, 5 μm. **b** Comparison of resolution of confocal and STED MAP4-nirFAST680 micrographs using image decorrelation analysis[19] ($n = 8$ cells). **c** Enhancement of resolution of MAP4-nirFAST600 micrographs, calculated as the ratio between confocal resolution and STED resolution from (**b**). **e** Comparison of resolution of confocal and STED MAP4-nirFAST680 micrographs using image decorrelation analysis[19] ($n = 8$ cells). **f** Enhancement of resolution of MAP4-nirFAST680 micrographs, calculated as the ratio between confocal resolution and STED resolution from (**e**). See Supplementary Table 8 for detailed imaging settings and methods section for image decorrelation analysis parameters. Source data are provided as a Source Data file.

A green-NIR fluorescent cell cycle indicator

Next, we took advantage of the orthogonality of nirFAST715 and pFAST540 to design a green-NIR fluorescent ubiquitination cell cycle indicator (FUCCI). Based on the fusion of two spectrally orthogonal fluorescent reporters to fragments of Geminin and Cdt1, two cell-cycle regulators whose levels inversely oscillate during the cell cycle, FUCCI indicators enable to identify the different phases of the cell cycle[22]. While the use of FP-based FUCCI was generalized to different types of organisms, the study of short cell cycles remains highly challenging because of the slow fluorescence maturation of FPs. An alternative relies on the use of fast-activated fluorescent chemogenetic reporters such as FAST variants[23]. We reasoned that the use of pFAST and nirFAST, which both show quasi-instantaneous labeling (provided that their fluorogens are present), could allow the design of cell cycle indicator (hereafter named ^{FAST}FUCCI) circumventing the limitation of FP-based FUCCI. nirFAST was fused to the N-terminus domain of zCdt1(1–190) and pFAST was fused to the N-terminus of zGeminin(1–100). Cdt1 and Geminin are substrates of the two complexes SCF^{Skp2} and APC^{Cdh1}, which display cell cycle phase-dependent activities. These two complexes are involved in the tight control of DNA replication, which occurs during the S phase of the cycle. In particular, geminin is degraded during G1 while Cdt1 is degraded during S/G2/M. Thus, fluorescent reporters fused to fragments of Cdt1 and Geminin can directly report the accumulation or degradation of these two proteins, allowing the delineation of cell cycle phases[22]. Long-term timelapse imaging of HEK293T cells showed that ^{FAST}FUCCI enabled to report on the different stages of the cell cycle, while having no deleterious effect on cell viability and division (Supplementary Fig. 13 and Supplementary Movie 3). The observation of asynchronized cells revealed several types of transitions (Fig. 6 and Supplementary Movie 4). Cells right after division displayed NIR fluorescence, in agreement with the accumulation of Cdt1 during the G1 phase. Over time, the NIR signal decreased while the green fluorescence increased with an overlap of the two signals, revealing a transition to the S phase. The full disappearance of the NIR fluorescence and constant green fluorescent signal allowed us to identify cells

https://doi.org/10.1038/s41467-025-58017-9

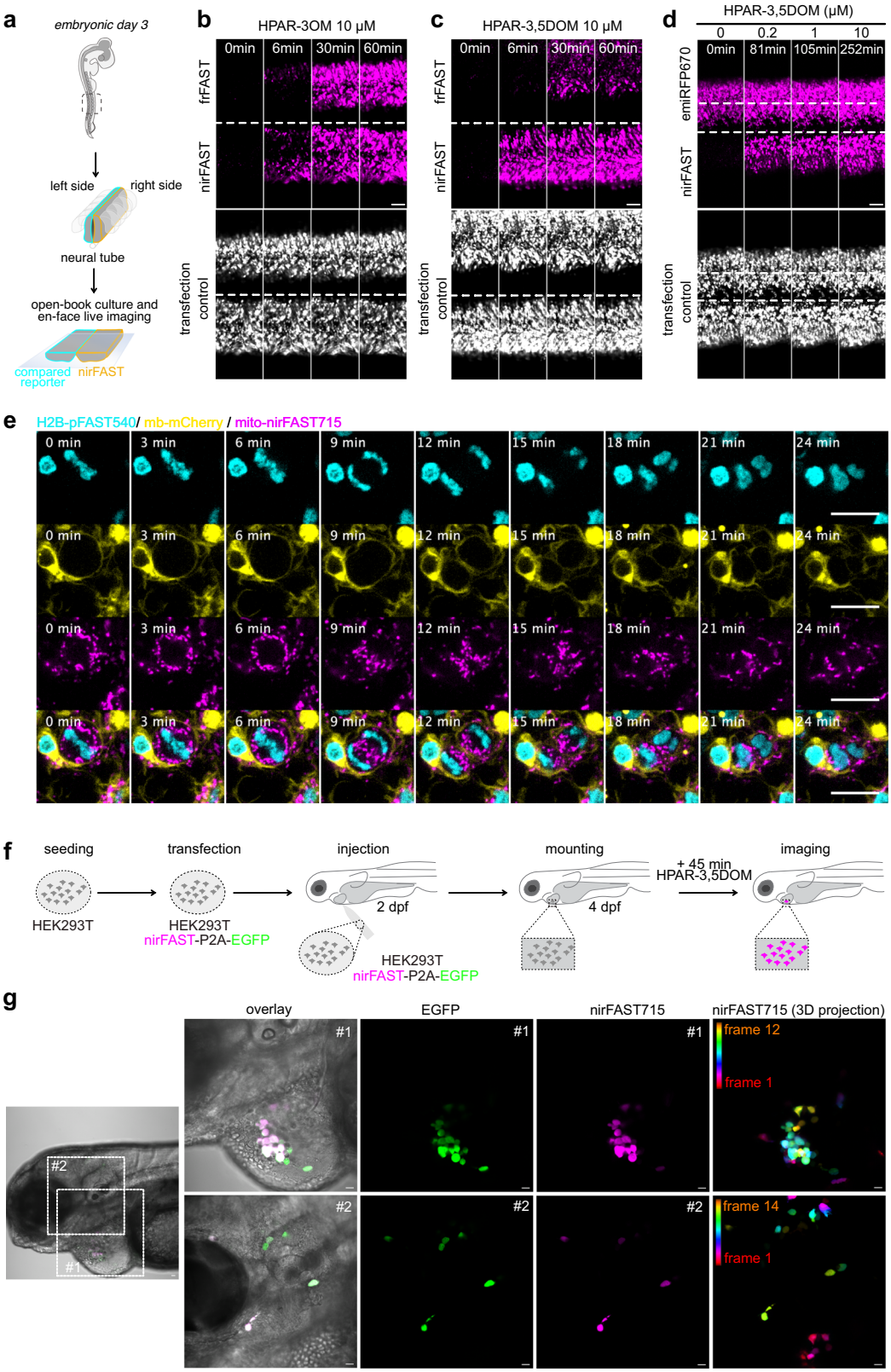

having reached the G2 phase. ^{FAST}FUCCI, thus, is a suitable indicator for delineating different phases of the cell cycle with green and NIR readout.

Control of protein proximity using bisected nirFAST

Bisection of fluorescent reporters in two complementary fragments is a general approach for the development of methods to image or control the proximity of proteins[24]. Using the split site 114–115 previously used for splitting FAST variants[25–27], we split-nirFAST into two complementary fragments dubbed nirFAST$_{1\text{-}114}$ and nirFAST$_{115\text{-}125}$. We evaluated the complementation of this split system (dubbed split-nirFAST) by fusing nirFAST$_{1\text{-}114}$ to the C-terminus of the FKBP-rapamycin-binding domain (FRB) of the mechanistic target of rapamycin (mTOR), and nirFAST$_{115\text{-}125}$ to the C-terminus of the FK506-

https://doi.org/10.1038/s41467-025-58017-9

Fig. 5 | Selective imaging of nirFAST in chicken embryo and zebrafish larvae. **a**–**c** Plasmids encoding nirFAST-P2A-EGFP and frFAST-P2A-EGFP were electroporated in each side of the neural tube in ovo at embryonic day 2. 24 h later, embryos with homogenous bilateral reporter expression in the neural tube were dissected and imaged upon the addition of 10 μM of HPAR-3OM or HPAR-3,5DOM by timelapse spinning disk microscopy. Scale bars 100 μm. Representative timelapse micrographs of $n = 3$ independent experiments. **d** Plasmids encoding nirFAST-P2A-EGFP and emiRFP670-P2A-EGFP were electroporated in each side of the neural tube in ovo at embryonic day 2. Twenty-four hours later, embryos with homogenous bilateral reporter expression in the neural tube were dissected and the neuroepithelium was imaged in en-face view by timelapse spinning disk microscopy upon sequential addition of 0.2, 1, and 10 μM HPAR-3,5DOM. Scale bars 100 μm. Representative micrographs of $n = 3$ independent experiments. **e** Plasmids encoding H2B-pFAST (cyan), memb-mCherry (yellow) and mito-nirFAST (magenta) were electroporated in the neural tube in ovo, at embryonic day 2 (E2, HH stage 13–14). Twenty-four hours later, embryos were dissected, and the neuroepithelium was imaged in en-face view in the presence of 1 μM HMBR (to assemble pFAST540) and 10 μM HPAR–3,5DOM (to assemble nirFAST715) using a spinning disk microscope (see also Supplementary Movie 2). Scale bars, 10 μm. Representative micrographs of $n = 3$ independent experiments. **f**, **g** Mammalian HEK293T were transfected with plasmid encoding nirFAST-P2A-EGFP. After 24 h, they were injected near the heart of 2 dpf zebrafish larvae. Larvae with green fluorescence signal were selected and imaged at 4 dpf after 45 min incubation with HPAR-3,5DOM (to assemble nirFAST715). Representative micrographs of $n = 3$ independent experiments. Scale bars, 20 μm. See Supplementary Table 8 for detailed imaging settings.

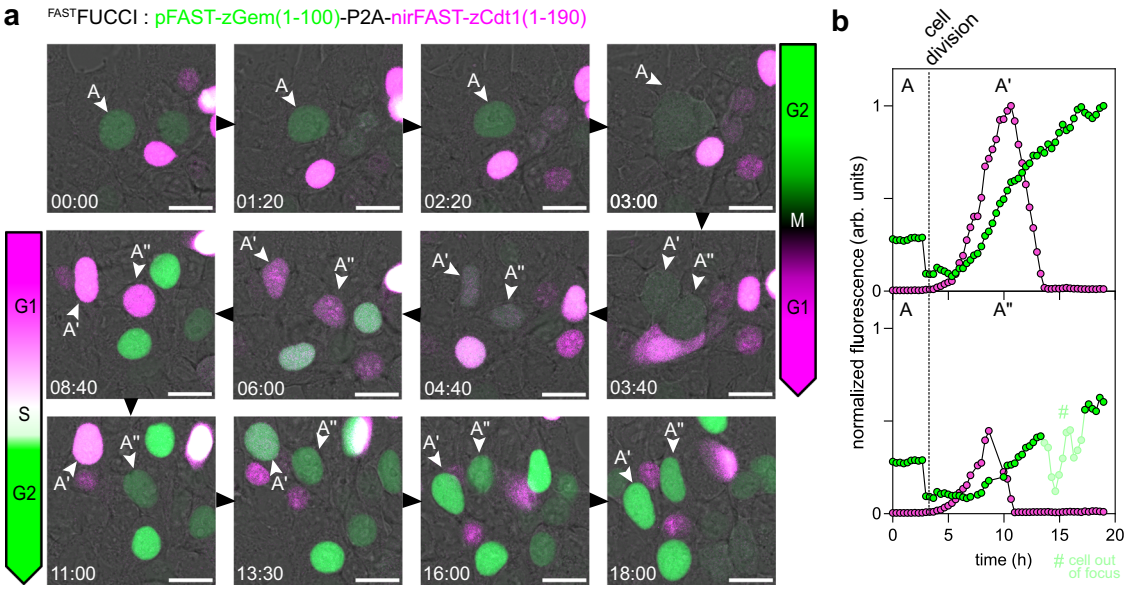

Fig. 6 | FASTFUCCI, a green-NIR fluorescent chemogenetic cell-cycle indicator. **a** HEK293T cells expressing FASTFUCCI and treated with 1 μM HMBR (to assemble pFAST540) and 10 μM HPAR-3,5DOM (to assemble nirFAST715) were imaged by timelapse confocal microscopy (1 frame every 20 min) for 24 h. Relevant timepoints of the designated field of view are shown to highlight transitions between the different cell cycle stages. Representative micrographs from three independent experiments (see also Supplementary Movie 4). **b** Fluorescence intensity evolution of tracked cell (cell A), which upon mitosis gives cells A′ and cells A″, is shown over time. Cell tracking and lineage was achieved through the Trackmate plugin (Fiji)[41,42]. See Supplementary Table 8 for detailed imaging settings. Source data are provided as a Source Data file.

binding protein (FKBP). As FKBP and FRB interact in the presence of rapamycin[28], the quantification of NIR fluorescence without and with rapamycin allowed us to quantify the efficiency of complementation of split-nirFAST in the absence and in the presence of interaction at various fluorogen concentrations (Supplementary Fig. 14). Flow cytometry analysis revealed that split-nirFAST displayed efficient complementation in cells with both HPAR-3OM and HPAR-3,5DOM regardless of the presence of rapamycin (Supplementary Fig. 14a, b, e). Similarly to what was observed for other split-FASTs, self-complementation of the ternary fluorescent assembly increases with fluorogen concentration. The high self-complementation of split-nirFAST680 and split-nirFAST715 in cells was also observed by confocal microscopy (Supplementary Fig. 14c, d, f, g).

Although high self-complementation precluded the use of split-nirFAST680 or split-nirFAST715 as a reporter of protein–protein interactions, this behavior could be leveraged to chemically induce protein proximity using the recently described CATCHFIRE (chemically assisted tethering of chimera through fluorogenic induced recognition) approach. CATCHFIRE uses FIREmate (a.k.a. $pFAST_{1\text{-}114}$) and FIREtag (a.k.a. $pFAST_{115\text{-}125}$) as dimerization domains that can interact together in the presence of various fluorogens (a.k.a. "matches")[27]. $nirFAST_{115\text{-}125}$ and FIREtag only differ by one mutation at position 117 (S117R). Characterization of full-length $nirFAST^{S117R}$ showed that this variant conserved good affinity for HPAR fluorogens (Supplementary Table 7). We showed that the replacement of $nirFAST_{115\text{-}125}$ by FIREtag did not hamper fluorogen-induced complementation. Co-expression in HEK293T cells of FRB-$nirFAST_{1\text{-}114}$ along with mCherry-$nirFAST_{115\text{-}125}$ or mCherry-FIREtag, respectively, allowed us to demonstrate that fluorogen-induced complementation was more efficient with FIREtag than with $nirFAST_{115\text{-}125}$ (Supplementary Fig. 15). Optimal fluorogen-induced complementation was observed when combining $nirFAST_{1\text{-}114}$, FIREtag and HPAR-3,5DOM (Supplementary Fig. 15b, f–h).

This set of experiments suggested the possibility to control the proximity of two proteins with a NIR fluorescence readout using $nirFAST_{1\text{-}114}$ (hereafter called nir-FIREmate) and FIREtag as dimerizing domains and HPAR fluorogens as fluorogenic inducers of proximity, and we called the resulting system nirCATCHFIRE. We fused nir-FIREmate to the C-terminus of the N-terminal domain of the mitochondrial outer membrane protein TOM20 ($TOM20_{1\text{-}34}$) and co-expressed it with EGFP-FIREtag in HeLa cells (Fig. 7a). Correct localization of nir-FIREmate fusion at the mitochondria was assessed through insertion of the enhanced cyan fluorescent protein (ECFP). In the absence of fluorogen, EGFP-FIREtag displayed cytosolic localization, demonstrating the absence of complementation of nir-FIREmate and FIREtag in the absence of

https://doi.org/10.1038/s41467-025-58017-9

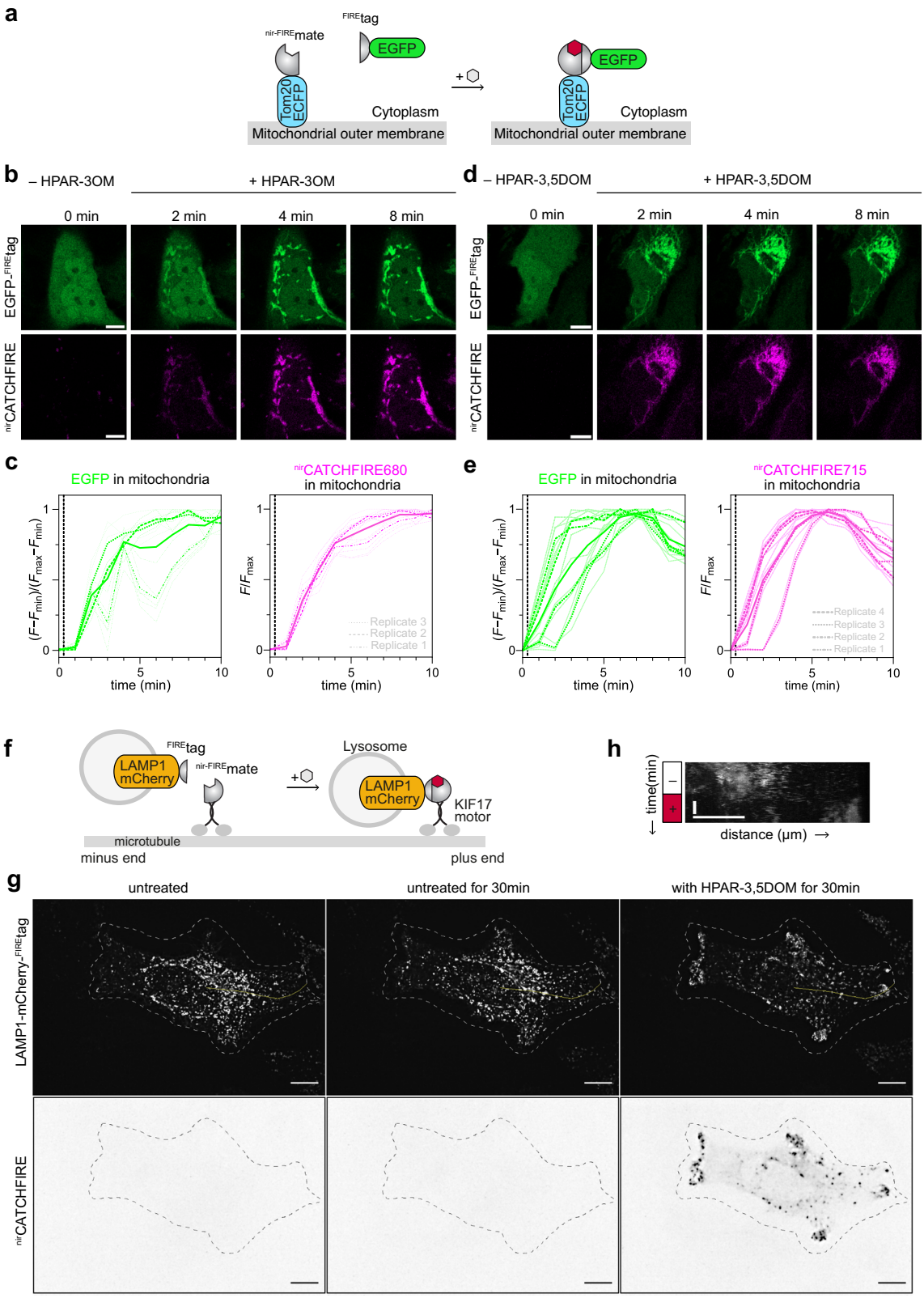

fluorogen. The addition of HPAR-3OM or HPAR-3,5DOM induced the rapid translocation of the green fluorescent EGFP-FIREtag from the cytosol to the surface of the mitochondria and the formation of the ternary complex between nir-FIREmate, FIREtag, and the fluorogen, as evidenced by an increase of the green fluorescence signal and NIR signal at the outer membrane of mitochondria in timelapse confocal microscopy experiments (Fig. 7b, d and Supplementary Movies 5, 6). NIR signal reached 50% of maximum fluorescence two to three minutes after fluorogen addition, demonstrating fast fluorogen-induced association of nir-FIREmate and FIREtag (Fig. 7c, e).

To demonstrate the possibility of controlling cellular processes, we applied nirCATCHFIRE to control the positioning of lysosomes (Fig. 7f). nir-FIREmate was fused to the C-terminus of the motor domain of kinesin-like KIF17, while FIREtag was fused to lysosomal-associated

Fig. 7 | ^{nir}CATCHFIRE: a fluorogenic chemically induced dimerization tool with NIR fluorescence readout. a Schematic illustrating the fluorogen-induced interaction between EGFP-^{FIRE}tag and Tom20-ECFP-$^{nir\text{-}FIRE}$mate for chemically induced recruitment at the outer mitochondrial membrane. **b**–**e** HeLa cells co-expressing EGFP-^{FIRE}tag together with Tom20-ECFP-$^{nir\text{-}FIRE}$mate were treated with 10 μM of either HPAR-3OM (**b**, **c**) or HPAR−3,5DOM (**d**, **e**), and imaged by timelapse confocal microscopy. **b**, **d** Representative confocal micrographs before and after the addition of the fluorogen (see also Supplementary Movies 5, 6). Scale bar 10 μm. **c**, **e** Temporal evolution of the mitochondrial EGFP and ^{nir}CATCHFIRE fluorescence of (**c**) $n = 15$ cells (from three independent experiments) and (**d**) $n = 14$ cells (from four independent experiments). The dashed line indicates fluorogen addition. **f** Schematic illustrating how fluorogen-induced interaction between LAMP1−mCherry−^{FIRE}tag and $^{nir\text{-}FIRE}$mate−KIF17 allows the chemically induced anterograde transport of lysosomes. **g** HeLa cells co-expressing LAMP1−mCherry−^{FIRE}tag and $^{nir\text{-}FIRE}$mate−KIF17 were imaged by spinning disk microscopy for 30 min, then HPAR−3,5DOM was added. Representative micrographs of each step (see also Supplementary Movie 7). Experiments were repeated three times with similar results. Scale bars 10 μm. **h** Kymograph showing the LAMP1−mCherry−^{FIRE}tag along the yellow line in (**e**) over time. See Supplementary Table 8 for detailed imaging settings. Source data are provided as a Source Data file.

membrane protein (LAMP)1 at the surface of lysosomes. Co-expression of the two proteins in live cells allowed us to control lysosome positioning. The addition of HPAR-3,5DOM led to the displacement of lysosomes from the perinuclear region to the cell periphery, demonstrating the successful fluorogen-induced recruitment of the molecular motor (Fig. 7g, h and Supplementary Movie 7).

This set of experiments opens exciting prospects for controlling the localization and motion of proteins and organelles using the ^{nir}CATCHFIRE technology. Its NIR fluorescence properties offer the additional advantage of possibly reporting additional biological events using green or red-emitting reporters.

Discussion

NIR fluorescent reporters allow observations in living tissues with high contrast and lower phototoxicity. The need for reporters that fully maximize the advantages of the NIR spectral window drove the development of a toolbox of NIR FPs for various applications in bioimaging[1–6]. In this work, we present the development of nirFAST, a NIR fluorescent chemogenetic reporter, made of a 14 kDa protein tag able to tightly bind and stabilize a new fluorogenic push-pull chromophore called HPAR-3,5DOM displaying efficient permeation across cell membranes. To engineer nirFAST, we took advantage of the bimodular nature of chemogenetic systems to conduct a concerted strategy of fluorogen and tag engineering. By altering the chromophore structure and refining the protein structure through two rounds of directed evolution, we maximized NIR fluorescence brightness, and obtained spectral properties finely adjusted to excitation at 633 nm or 640 nm readily available on most microscope setups.

Although nirFAST was engineered and optimized to take advantage of the benefits of NIR excitation and emission, efficient binding and fluorescence activation can also be achieved with HPAR-3OM yielding far-red fluorescence (nirFAST680), and HBR-3,5DOM yielding red fluorescence (nirFAST600). The fluorescence of nirFAST can thus be finely tuned from red to NIR only by changing the fluorogen, highlighting the versatility and high tunability of chemogenetic systems.

nirFAST680 and nirFAST715 were shown to be brighter than the spectrally equivalent top-performing NIR FPs emiRFP670 and miRFP713 in cultured mammalian cells. As their fluorescence is only reliant on the addition of highly permeant exogenous fluorogens, they can be used as effective alternatives of NIR FP in a variety of biological contexts where scarce levels of biliverdin hamper their use (e.g. neurons[29]). nirFAST displays the additional advantage of being half the size of the top-performing NIR FPs, opening interesting prospects for labeling proteins with robust fluorescence and minimal perturbation. Finally, full labeling of nirFAST in cells is achieved within seconds of fluorogen addition, indicating that the rate of labeling is primarily constrained by fluorogen cell uptake and diffusion. This means that in cells pre-treated with the fluorogen, labeling is nearly instantaneous, which should enable the reporting of dynamic and rapid biological processes such as protein neosynthesis and turnover. This contrasts with biliverdin-based NIR FPs, which can be limited by their longer maturation time due to slower covalent incorporation of biliverdin[3].

In this study, we showed that nirFAST is advantageous for simultaneous imaging of several biological targets, as it can be combined with various fluorescent reporters emitting in the visible. In addition to being unmistakably distinguishable from widely used red-emitting fluorescent reporters due to its red-shifted spectral properties, nirFAST is also orthogonal to pFAST, another chemogenetic reporter of the FAST family capable of yielding green fluorescence. nirFAST allowed spectral multiplexed imaging in cells as well as in chicken embryo tissues, where the dynamics of three subcellular proteins were simultaneously monitored during cell division.

The orthogonality of nirFAST and pFAST allowed the design of a FUCCI-like cell cycle indicator delineating cell-cycle stages with green and NIR fluorescence readout. The photostability and low toxicity of the ^{FAST}FUCCI indicator allowed the visualization of M/G1, as well as G1/S/G2, transitions over long periods of time while having the red channel readily available for monitoring additional processes. Because of the quasi-instantaneous labeling of nirFAST and pFAST, the ^{FAST}FUCCI indicator should be ideal for the monitoring of very short cell cycles, such as those in the early stages of embryogenesis[23].

In addition to requiring less toxic light for imaging, NIR fluorescent reporters facilitate imaging in biological tissues, which are less autofluorescent in this spectral window, enabling thus observations without interference from inherent fluorescent structures. In this context, nirFAST enabled unambiguous high-contrast observation of injected cells inside zebrafish larvae. In these experiments we used non-tumorigenic HEK293T cells as a proof of concept of the successful labeling of injected cells inside zebrafish larvae. The advantageous spectral properties of nirFAST should allow its combination with the variety of existing EGFP-expressing transgenic zebrafish lines for the study of angiogenesis or response to anti-cancer drugs of tumorigenic injected cells.

While red, FR, and NIR lights are associated with better in-depth penetration and lower phototoxicity, they are often linked to lower spatial resolution in microscopy. In this study, we showed that the good spectral properties, photostability, and brightness of nirFAST600 and nirFAST680 make them well-suited reporters for STED, and enable live-cell subdiffraction imaging of fine cellular structures such as microtubules with a 1.6-fold resolution enhancement.

Finally, we used nirFAST to design a fluorogenic chemically inducible dimerization tool with NIR fluorescence readout. The bisection of members of the FAST family previously led to chemogenetic tools enabling the functional study of protein−protein interactions[10,23,25–27]. Bisection led to either systems displaying low self-complementation in the presence of the fluorogen, well suited for reporting protein−protein interactions[26] and contact sites between organelles[30,31] or to systems displaying high self-complementation in the presence of the fluorogen, which were used to develop CATCHFIRE (chemically assisted tethering of chimera through fluorogenic induced recognition)[27], a chemically induced dimerization tool with intrinsic fluorescence readout for controlling and visualizing protein proximity. Bisection of nirFAST allowed us to generate a CATCHFIRE system with NIR fluorescence readout, dubbed ^{nir}CATCHFIRE, in which HPAR-3OM and HPAR-3,5DOM act as fluorogenic molecular glues promoting the

dimerization of the two fragments. This system can thus be used to chemically control and also visualize the proximity of two proteins fused to the two fragments.

Either used in its full-length or split version, nirFAST opens exciting prospects for the development of novel single wavelength or FRET-based tunable biosensors with NIR readout for unraveling biological processes in complex model organisms. We expect the promising properties of nirFAST to make it an interesting addition to the existing toolbox of NIR fluorescent reporters.

Methods

Ethical statement

The presented research complies with all relevant ethical regulations. For the zebrafish experiments, the animal facility obtained permission from the French Ministry of Agriculture (agreement No. D-75-05-32.) and all animal procedures were performed in accordance with French animal welfare guidelines. For chicken embryo tissue experiments, JA57 chicken fertilized eggs were provided by EARL Morizeau (8 rue du Moulin, 28190 Dangers, France) and incubated at 38 °C in a Sanyo MIR-253 incubator. Embryos used in this study were between E2 (HH14) and E3 (HH14 + 24 h). The sex of the embryos was not determined. Under current European Union regulations, experiments on avian embryos between 2 and 4 days in ovo are not subject to restrictions.

Organic synthesis

General. Commercially available reagents were used as obtained. ^{1}H and ^{13}C NMR spectra were recorded at 300 K on a Bruker AM 300 spectrometer; chemical shifts are reported in ppm with protonated solvent as internal reference; coupling constants *J* are given in Hz. Mass spectra were performed by the Service de Spectrométrie de Masse de Chimie Paris Tech (France). The synthesis of HPAR-3OM[10], HBR-3,5DOM[14], HBR-3,5DM[14] and HMBR[13] was previously reported. These fluorogens are commercially available from the Twinkle Factory under the names ^{TF}Poppy, ^{TF}Coral, ^{TF}Amber, and ^{TF}Lime.

HPAR-3,5DOM ((Z)-5-((E)-3-(4-hydroxy-3,5-dimethoxyphenyl)allylidene)-2-thioxothiazolidin-4-one. To a stirred solution of rhodanine (133 mg, 1.0 mmol) and 4-hydroxy-3,5-dimethoxycinnamaldehyde (208 mg, 1.0 mmol) in ethanol (3 mL) was added 4-dimethylaminopyridine (12 mg, 0.11 mmol). The solution was stirred at reflux for 20 h. The solution was neutralized by adding 1 N HCl. After cooling to 4 °C and standing overnight, the precipitate was filtered, and the crude solid was washed with EtOH/H_2O 1:5. HPAR-3,5DOM was obtained as a red powder (303 mg, 94% yield). ^{1}H NMR (300 MHz, CD_3SOCD_3, δ in ppm): 13.55 (s, 1H), 9.08 (s, 1H), 7.32 (d, J = 11.7 Hz, 1H), 7.21 (d, J = 15.0 Hz, 1H), 6.99 (s, 2H), 6.91 (dd, J = 11.7, 15.0 Hz, 1H), 3.82 (s, 6H). ^{13}C NMR (75 MHz, CD_3SOCD_3, δ in ppm): 195.2, 168.7, 148.1(2 C), 146.3, 138.5, 133.1, 126.2, 124.6, 121.2, 106.1(2 C), 56.2(2 C). MS (ESI): m/z 322.3 $[M-H]^-$ (calculated mass for $[C_{14}H_{12}NO_4S_2]^-$: 322.3).

Biology

General. Synthetic oligonucleotides used for cloning were purchased from Integrated DNA Technology. PCR reactions were performed with Q5 polymerase (New England Biolabs) in the buffer provided. PCR products were purified using a QIAquick PCR purification kit (QIAGEN). DNase I, T4 ligase, fusion polymerase, Taq ligase and Taq exonuclease were purchased from New England Biolabs and used with accompanying buffers and according to the manufacturer's protocols. Isothermal assemblies (Gibson Assembly) were performed using a homemade mix prepared according to previously described protocols[32]. Small-scale isolation of plasmid DNA was conducted using a QIAprep miniprep kit (QIAGEN) from 2 mL overnight bacterial culture supplemented with appropriate antibiotics. Large-scale isolation of plasmid DNA was conducted using the QIAprep maxiprep kit (QIAGEN) from 150 mL overnight bacterial culture supplemented with appropriate antibiotics. All plasmid sequences were confirmed by Sanger sequencing with appropriate sequencing primers (GATC Biotech). All the plasmids used in this study are listed in Supplementary Table 9, as well as DNA sequences. The construction of the combinatorial libraries for the directed evolution of nirFAST, as well as the screening protocol by FACS, are described in Supplementary Methods.

Cloning. The plasmids used in this study have been generated using isothermal Gibson Assembly or restriction enzyme cloning. The construction of the plasmids for the characterization of clones from the directed evolution experiments is described in Supplementary Methods.

Plasmid pAG1253 for bacterial expression of 6×His–TEVcs–nirFAST under the control of a T7 promoter was obtained by introducing R52K mutation in the sequence coding for nirFAST2.0 (see Supplementary Methods).

Plasmids for mammalian expression of emiRFP670 and miRFP713 under the control of CMV promoter were obtained from Addgene vectors #136556 and #136559. Plasmids pAG1329, pAG1334, pAG1335, and pAG1337 for mammalian expression of nirFAST-P2A-EGFP-cMyc, frFAST-P2A-EGFP-cMyc, emiRFP670-P2A-EGFP-cMyc and miRFP713-P2A-EGFP-cMyc respectively were obtained by replacement of the sequence of FAST by the sequences of nirFAST, frFAST, emiRFP670 and miRFP713 respectively in the plasmid pAG453 coding for FAST-P2A-EGFP (not published). The plasmid pAG1371 for mammalian expression of nirFAST under the control of a CMV promoter was obtained by replacing the sequence of frFAST with that of nirFAST in plasmid pAG504[10] encoding frFAST. The plasmid pAG1372 for mammalian expression of H2B-nirFAST-cMyc was obtained by replacing the sequence of pFAST with nirFAST in the plasmid pAG657 for mammalian expression of H2B-pFAST[9]. The plasmid pAG1375 for mammalian expression of mito-nirFAST-cMyc was obtained by replacing the sequence of pFAST with that of nirFAST in the plasmid pAG671[9] for the expression of mito-pFAST-cMyc. Similarly, the plasmid pAG1380 for mammalian expression of MAP4-nirFAST-cMyc was obtained by replacing the sequence of pFAST with that of nirFAST in plasmid pAG665[9] for mammalian expression of MAP4-pFAST. The plasmid pAG1377 for mammalian expression of nirFAST-Cb5 was obtained by replacing the sequence of $FAST_{1\text{-}114}$-eCFP with the sequence of nirFAST in the plasmid pAG1168 (not published) for mammalian expression of $FAST_{1\text{-}114}$-ECFP-Cb5. Plasmids pAG1329 (nirFAST-P2A-EGFP-cMyc), pAG1334 (frFAST-P2A-EGFP-cMyc), pAG1335 (emiRFP670-P2A-EGFP-cMyc) and pAG1337 (miRFP713-P2A-EGFP-cMyc) described above were used for characterization of nirFAST properties at low magnification in chicken embryo tissues. For imaging of mito-nirFAST at high magnification in the chick neural tube, the CMV promotor in pAG1375 was replaced by the CAGGS promoter from pCAGGS-zH2B-frFAST[10]. The plasmid for expression of pCAGGS-zH2B-pFAST for expression of H2B-pFAST in chicken embryo was previously described[9]. The plasmid X-159 for expression of membrane-localized memb-mCherry in chicken embryo was previously described[33]. ^{FAST}FUCCI (pSV1363) was obtained (via NEBuilder DNA Assembly) in two steps, first replacing the sequence of greenFAST by the sequence of nirFAST upstream zCdt1(1–190) in pSV1135 coding for redFAST-zGem(1–100)-P2A-greenFAST-zCdt1(1–190)[23], then replacing in the resulting plasmid the sequence of redFAST by the sequence of pFAST upstream zGeminin(1–100). The plasmid pAG721 for the mammalian expression of lyn11-mCherry was obtained by Gibson assembly, by replacing the sequence of FAST by the sequence of mCherry in plasmid pAG106 for encoding lyn11-FAST and was used in a previous study[9]. The plasmid pAG1171 for encoding ^{FIRE}mate-ECFP-giantin used in this study for the expression of ECFP at the Golgi apparatus was previously described[27]. The plasmid pAG324 used for encoding H2B-mCherry used in this study for the expression of mCherry in the nucleus was previously

described[10]. The plasmid pAG506 used for encoding mito-frFAST was previously described[10].

The plasmid pAG1384 for mammalian expression of FKBP-nirFAST$_{115\text{-}125}$-IRES-EGFP was obtained by replacing the sequence of iRFP670 with the sequence of EGFP in the plasmid pAG577[26] for mammalian expression of FKBP-FAST$_{115\text{-}125}$-IRES-iRFP670. The plasmid pAG1385 for mammalian expression of FRB-nirFAST$_{1\text{-}114}$-IRES-mTurquoise2 was obtained from the plasmid pAG490[26] for mammalian expression of FRB-FAST$_{1\text{-}114}$-IRES-mTurquoise2 by replacing the sequence of FAST$_{1\text{-}114}$ by the sequence of nirFAST$_{1\text{-}114}$. The plasmid pAG1501 for mammalian expression of TOM20-ECFP-nirFAST$_{1\text{-}114}$ was obtained by replacing the sequence of FRB with the sequence of nirFAST$_{1\text{-}114}$ in Addgene plasmid #171461 for mammalian expression of TOM20-ECFP-FRB(2021-2113 aa). The plasmid KIF17MD-flag-$^{\text{nir-FIRE}}$mate was constructed by insertion of the $^{\text{nir-FIRE}}$mate from the plasmid pAG1501 encoding TOM20-ECFP-nirFAST$_{1\text{-}114}$ in a vector for the expression of KIF17MD-flag-FIREmate (pFP5370)[27].

In silico modeling of nirFAST

The homology models of nirFAST and frFAST were generated according to models previously described[34,35]. Briefly, sequence alignments between nirFAST and frFAST and the ultra-high resolution structure of the *Halorhodospira halophila* Photoactive Yellow Protein (PYP) as well as FAST 3D NMR structures (Protein Data Bank (PDB) ID: 6P4I, 7AV6, 7AVA, 7AVB[36,37]) were generated with Clustal W[38]. Alignments were manually refined. Three-dimensional nirFAST and frFAST models were built from these alignments and from crystallographic atomic coordinates of PYP using the automated comparative modeling tool MODELER (Sali and Blundell) implemented in Discovery Studio. The best model according to the DOPE score (Discrete Optimized Protein Energy) and potential energy calculated by the modeler were solvated with a minimum distance from the periodic boundary of 10 Å (water and 0.145 M NaCl) and minimized using the Adopted Basis NR algorithm to a final gradient of 0.001. The resulting structure were submitted to a 10 ns NAMD dynamics. Time course analysis has been performed by following RMSD/RMSF/electrostatic energy evolution.

Flexible ligand-rigid protein docking was performed using CDOCKER implemented in Discovery Studio 2020[39]. Random ligand conformations were generated from the initial ligand structure through high-temperature molecular dynamics. The best poses according to their ligscore2[40] were retained and clustered according to their binding mode. The most significant poses were solvated and minimized using Adopted Basis NR algorithm to a final gradient of 0.001. The resulting structure were submitted to a 10 ns NAMD dynamics. Time course analysis has been performed by following RMSD/RMSF/electrostatic energy evolution.

RMSD and RMSF are shown on Supplementary Fig. 6. Coordinate files of the initial input and final output are provided as Supplementary Data.

Cell culture. HeLa cells (ATCC CRM-CCL2) were cultured in minimal essential medium supplemented with phenol red, Glutamax I, 1 mM of sodium pyruvate, 1% (vol/vol) of non-essential amino acids, 10% (vol/vol) fetal bovine serum (FBS) and 1% (vol/vol) penicillin–streptomycin at 37 °C in a 5% CO_2 atmosphere. HEK293T (ATCC CRL-3216) cells were cultured in Dulbecco's modified Eagle medium (DMEM) supplemented with phenol red, 10% (vol/vol) FBS, and 1% (vol/vol) penicillin–streptomycin at 37 °C in a 5% CO_2 atmosphere. For imaging, cells were seeded in µDish IBIDI (Biovalley) coated with poly-L-lysine. Cells were transiently transfected using Genejuice (Merck) according to the manufacturer's protocols for 24 h before imaging. Cells were washed with Dulbecco's PBS (DPBS) and treated with DMEM (without serum and phenol red) supplemented with the compounds at the indicated concentration.

Cell viability assay. HeLa and HEK293T cells were treated with the indicated fluorogens concentrations for 24 h. The cell viability was assessed using the Celltiter-Glo kit (Promega) through measurement of the luminescence signal on a PolarStar Optima plate-reader (BMG Labtech) according to manufacturer's protocol.

Protein expression in bacteria and purification. Plasmids were transformed in BL21 (DE3) competent *Escherichia coli* (New England Biolabs) or Rosetta (DE3) pLysS *E. coli* (Merck). Cells were grown at 37 °C in a lysogen broth medium supplemented with 50 µg.mL^{-1} kanamycin (and 34 µg.mL^{-1} of chloramphenicol for Rosetta) to OD_{600nm} 0.6. Expression was induced overnight at 16 °C by adding isopropyl β-D-1-thiogalactopyranoside (IPTG) to a final concentration of 1 mM. Cells were collected by centrifugation (4300×*g* for 20 min at 4 °C) and frozen. For purification, the cell pellet was resuspended in lysis buffer (PBS supplemented with 2.5 mM $MgCl_2$, 1 mM of protease inhibitor phenylmethanesulfonyl fluoride, and 0.025 mg.mL^{-1} DNase, pH 7.4) and sonicated (5 min, 20% of amplitude) on ice. The lysate was incubated for 2 h on ice to allow DNA digestion by DNase. Cellular fragments were removed by centrifugation (9000×*g* for 1 h at 4 °C). The supernatant was incubated overnight at 4 °C by gentle agitation with prewashed Ni-NTA agarose beads in PBS buffer complemented with 20 mM of imidazole. Beads were washed with ten volumes of PBS complemented with 20 mM of imidazole and with five volumes of PBS complemented with 40 mM of imidazole. His-tagged proteins were eluted with five volumes of PBS complemented with 0.5 M of imidazole. The buffer was exchanged to PBS (0.05 M phosphate buffer and 0.150 M NaCl) using PD-10 desalting columns or Midi-Trap G-25 (GE Healthcare). The purity of the proteins was evaluated using SDS–PAGE electrophoresis stained with Coomassie blue.

Physicochemical measurements. Steady-state UV-Vis and fluorescence spectra were recorded at 25 °C on a Spark 10 M (Tecan). Data were processed using GraphPad Prism v.10.0.3. Fluorescence quantum yield measurements were determined in 96-well plates using either FAST:HBR-3,5DOM or frFAST:HPAR-3OM as a reference. Solutions of 40 µM of proteins were used, in which the fluorogen was diluted to the right concentration, usually from 6 µM to 0.375 µM, allowing >99% of complex formation. Absorption coefficients were determined directly by the previous experiments after the determination of the optical path length. Thermodynamic dissociation constants were determined by titration experiments in which we measured the fluorescence of the fluorescent assembly at various fluorogen concentrations using a Spark 10 M plate reader (Tecan) and fitting data in GraphPad Prism 9 to a one-site specific binding model[9–14,23] Detailed derivation of the thermodynamic dissociation constants can be found in ref. 13 and the protocol of their measurement is detailed in ref. 12. In brief, the dissociation constant of the fluorogen:protein assembly is determined by titration experiment in a 96-well plate format. As the fluorogen:protein assembly is strongly fluorescent, one can directly use fluorescence as a readout to determine the fraction of the complex. Titrations are performed varying the fluorogen concentration while keeping the protein concentration constant. Measurement of the fluorescence intensity at each fluorogen concentration enables to quantify the fraction of complex. These experiments are done in large molar excess of fluorogen to be able to neglect the variation of free fluorogen concentration upon complex formation. We used protein concentrations of 35–50 nM. To determine the specific signal from the complex, the contribution of the free fluorogen (baseline) was measured and subtracted. We used twelve different concentrations of fluorogen. The fluorescence titration data were analyzed by fitting with a one-site specific binding model using GraphPad Prism 9 software.

Flow cytometry analysis. Flow cytometry analysis of HEK293T cells was performed on a MACSQuant analyzer equipped with 405, 488, and

635 nm lasers and seven channels. To prepare samples, cells were first grown in cell culture flasks, then transiently co-transfected 24 h after seeding using Genejuice (Merck) according to the manufacturer's protocol for 24 h. After 24 h, cells were centrifuged in PBS with BSA (1 mg.mL^{-1}) and resuspended in PBS–BSA supplemented with the appropriate amounts of compounds. For each experiment, 20,000 cells positively expressing mTurquoise2 (Ex 405 nm/ Em 425–475 nm) and EGFP (Ex 488 nm/Em 500–550 nm) or mCherry (Ex 488 nm/Em 565–605 nm) were analyzed with the following parameters: Ex 635 nm/ Em 655–730 nm. Data were analyzed using FlowJo v.10.7.1. A figure presenting the gating strategy is presented in Supplementary Fig. 16.

Fluorescence microscopy. The confocal micrographs of mammalian cells were acquired on an inverted Zeiss LSM 980 Laser Scanning Microscope equipped with a plan-apochromat 63× /1.4 NA oil immersion objective, a plan-apochromat 40×/1.4 oil immersion objective and a plan-apochromat 20×/0.8 dry objective and an inverted Leica TCS SP5 confocal laser scanning microscope equipped with a 63×/1.4 NA oil immersion objective. The confocal micrographs of zebrafish were acquired on an upright Zeiss LSM 980 Laser scanning microscope equipped with a plan-apochromat 20×/1.0 DIC (UV)VIS-IR M27 75 mm water objective. ZEN and Leica LAS AF softwares were used to collect the data. Icy and Fiji softwares were used to analyze the data. Fluorescence signal measurement was obtained through the Active Contour plugin on Icy. Lineage and tracking of dividing cells, as well as corresponding fluorescence signal extraction, was performed through Trackmate plugin[41,42] (Fiji).

Live imaging in the chick embryonic neuroepithelium was performed on an inverted microscope (Nikon Ti Eclipse) equipped with a heating enclosure (DigitalPixel, UK), a spinning disk confocal head (Yokogawa CSUW1) with Borealis system (Andor) and a sCMOS Camera (Orca Flash4LT, Hamamatsu) driven by MicroManager software[43]. Image stacks were obtained at 3-min intervals either with a 10× objective (CFI Plan APO LBDA, NA 0.45, Nikon) with a 5 μm z-step or a 100× oil immersion objective (APO VC, NA 1.4, Nikon) with a 0.3 μm z-step.

Confocal spinning disk images for control of lysosomes positioning were acquired on a Nikon Inverted Eclipse Ti-E (Nikon) microscope equipped with a Spinning disk CSU-X1 (Yokogawa), a Kinetx 22 sCMOS camera (Photometrics) integrated into Metamorph software by Gataca Systems, using a 100× CFI apochromat VC 1.4 NA oil immersion objective (Nikon). The images were analyzed with Fiji (Image J).

Super-resolution imaging. The comparative confocal and STED micrographs were acquired on the STEDYCON confocal and STED module (Abberior Instruments GmbH, Germany) connected to the lateral port of an IX83 inverted microscope (Evident Scientific). The STEDYCON SmartControl software was used for data acquisition. Imaging was performed using a UPLXAPO 100× oil immersion objective (Evident Scientific). The specimens were imaged with 561 nm (nirFAST600) or 640 nm (nirFAST680) lasers as well as a pulsed 775 nm depletion laser for STED imaging. Typically, images of 1024 × 1024 pixels were acquired with a pixel size in the range of 25–30 nm. Resolution assessment of confocal and STED images was performed using the image decorrelation analysis plugin in Fiji[19] using default parameters.

Zebrafish experiments

Adult zebrafish (*Danio rerio*) were kept at around 27–29 °C on a 14 h-light:10 h-dark cycle and fed twice daily. Natural crosses obtained fertilized eggs which were raised at 28 °C in Volvic water. Experiments were performed using the standard nacre strain. Developmental stages were determined and indicated as days post fertilization (dpf). The animal facility obtained permission from the French Ministry of Agriculture (agreement No. D-75-05-32.), and all animal procedures were performed in accordance with French animal welfare guidelines. HEK293T cells were seeded at 500,000 cells/mL concentration in 25 cm^2 flasks and transfected after 24 h with plasmid encoding nirFAST-P2A-EGFP using GeneJuice (Merck) according to manufacturer's guidelines. After 24 h, cells were harvested at 10,000,000 cells/mL concentration in serum-free DMEM.

The cell suspension was loaded into a borosilicate glass needle pulled by a Flaming/Brown micropipette puller (Narishige, Japan, PN-30). About 5–10 nL suspension were implanted into anesthetized (0.02% MS-222 tricaine (Sigma)) 2 dpf zebrafish larvae close to the heart by using an electronically regulated air-pressure microinjector (FemtoJet, Eppendorf). After injection, zebrafish larvae were placed in Volvic water and examined under a stereoscopic microscope for the presence of fluorescent cells and then raised for two more days at 28 °C before imaging. For imaging, living zebrafish larvae were anesthetized in MS-222 tricaine solution and embedded in a lateral orientation in low-melting agarose (0.8%). Larval zebrafish were studied before the onset of sexual differentiation, and their sex can therefore not be determined.

Chicken embryo experiments

JA57 chicken fertilized eggs were provided by EARL Morizeau (8 rue du Moulin, 28190 Dangers, France) and incubated at 38 °C in a Sanyo MIR-253 incubator. Embryos used in this study were between E2 (HH14) and E3 (HH14 + 24 h). The sex of the embryos was not determined. Under current European Union regulations, experiments on avian embryos between 2 and 4 days in ovo are not subject to restrictions.

In ovo electroporation in the chick neural tube was performed at embryonic day 2 (E2, HH stage 14), by applying five pulses of 50 ms at 25 V with 100 ms in between, using a square-wave electroporator (Nepa Gene, CUY21SC) and a pair of 5 mm gold-plated electrodes (BTW Genetrode model 512) separated by a 4 mm interval. The DNA solution was injected directly into the lumen of the neural tube via glass capillaries. Bilateral electroporation was achieved by switching the electrode's polarity and repeating the procedure after 3 h. DNA constructs were used at 1 μg/μL, except pCX-mbCherry which was used at 0.3 μg/μL; and pCX-zH2B-pFAST and pCX-mito-nirFAST which were used at 0.5 μg/μL. En-face culture of the embryonic neuroepithelium was performed at E3 (24 h after electroporation). After extraction from the egg and removal of extraembryonic membranes in PBS, embryos were transferred to 37 °C F12 medium and pinned down with dissection needles at the level of the hindbrain in a 35 mm Sylgard dissection dish. A dissection needle was used to slit the roof plate and separate the neural tube from the somites from the hindbrain to the caudal end on both sides of the embryo. The neural tube and notochord were then transferred in a drop of F12 medium to a glass-bottom culture dish (MatTek, P35G-0-14-C), and the medium was replaced with a 500 μL-1 mL of 1% low melting point agarose/F12 medium (maintained at 38 °C). Excess medium was removed so that the neural tube would flatten with its apical surface facing the bottom of the dish, in an inverted open-book conformation. After 30 s of polymerization on ice, an extra layer of agarose medium (200 μL) was added to cover the whole tissue and left to harden. 1.8 mL of 38 °C culture medium was added (F12/1 mM Sodium pyruvate), and the culture dish was transferred to the 38 °C chamber of a spinning disk confocal microscope. To image nirFAST, intermediate dilutions of ligands HPAR-3OM and HPAR-3,5DOM were prepared by diluting the original 20 mM stocks in F12 medium, and appropriate volumes were added to the dish to reach the desired final concentration.

Statistics and reproducibility

No sample size calculations were performed. When relevant, the sample size (n) is provided in the corresponding figure captions. Sample sizes were chosen to support meaningful conclusions. No data

were excluded. The number of replicates for each individual experiments is indicated in the figure legends. All attempts at replication were successful. The experiments were not randomized. The Investigators were not blinded to allocation during experiments and outcome assessment.

Reporting summary

Further information on research design is available in the Nature Portfolio Reporting Summary linked to this article.

Data availability

Data supporting the findings of this study are available within the article and supplementary information, and are available from the corresponding authors upon request. Requests will be fulfilled within four weeks. The plasmids developed in this study may be requested from the corresponding author. Source data are provided with this paper.

References

1. Shu, X. et al. Mammalian expression of infrared fluorescent proteins engineered from a bacterial phytochrome. *Science* **324**, 804–806 (2009).
2. Filonov, G. S. et al. Bright and stable near-infrared fluorescent protein for in vivo imaging. *Nat. Biotechnol.* **29**, 757–761 (2011).
3. Shcherbakova, D. M. et al Bright monomeric near-infrared fluorescent proteins as tags and biosensors for multiscale imaging. *Nat. Commun.* **7**, 12405 (2016).
4. Oliinyk, O. S., Shemetov, A. A., Pletnev, S., Shcherbakova, D. M. & Verkhusha, V. V. Smallest near-infrared fluorescent protein evolved from cyanobacteriochrome as versatile tag for spectral multiplexing. *Nat. Commun.* **10**, 1–13 (2019).
5. Shcherbakova, D. M., Stepanenko, O. V., Turoverov, K. K. & Verkhusha, V. V. Near-infrared fluorescent proteins: multiplexing and optogenetics across scales. *Trends Biotechnol.* **36**, 1230–1243 (2018).
6. Matlashov, M. E. et al. A set of monomeric near-infrared fluorescent proteins for multicolor imaging across scales. *Nat. Commun.* **11**, 239 (2020).
7. Zhang, H. et al. Quantitative assessment of near-infrared fluorescent proteins. *Nat. Methods* **20**, 1605–1616 (2023).
8. Oliinyk, O. S. et al. Deep-tissue SWIR imaging using rationally designed small red-shifted near-infrared fluorescent protein. *Nat. Methods* **20**, 70–74 (2023).
9. Benaissa, H. et al. Engineering of a fluorescent chemogenetic reporter with tunable color for advanced live-cell imaging. *Nat. Commun.* **12**, 6989 (2021).
10. Li, C. et al. A far-red emitting fluorescent chemogenetic reporter for in vivo molecular imaging. *Angew. Chem.* **132**, 18073–18079 (2020).
11. Gautier, A. Fluorescence-activating and absorption-shifting tags for advanced imaging and biosensing. *Acc. Chem. Res.* **55**, 3125–3135 (2022).
12. El Hajji, L., Benaissa, H. & Gautier, A. Isolating and engineering fluorescence-activating proteins using yeast surface sisplay. *Methods Mol. Biol.* https://doi.org/10.1007/978-1-0716-2285-8_25 (2022).
13. Plamont, M. A. et al. Small fluorescence-activating and absorption-shifting tag for tunable protein imaging in vivo. *Proc. Natl Acad. Sci. USA* **113**, 497–502 (2016).
14. Li, C. et al. Dynamic multicolor protein labeling in living cells. *Chem. Sci.* **8**, 5598–5605 (2017).
15. Saurabh, S., Perez, A. M., Comerci, C. J., Shapiro, L. & Moerner, W. E. Super-resolution imaging of live bacteria cells using a genetically directed, highly photostable fluoromodule. *J. Am. Chem. Soc.* **138**, 10398–10401 (2016).
16. Pimenta, F. M. et al. Chromophore renewal and fluorogen-binding tags: a match made to last. *Sci. Rep.* **7**, 1–8 (2017).
17. Kompa, J. et al. Exchangeable HaloTag ligands for super-resolution fluorescence microscopy. *J. Am. Chem. Soc.* **145**, 3075–3083 (2023).
18. Hell, S. W. & Wichmann, J. Breaking the diffraction resolution limit by stimulated emission: stimulated-emission-depletion fluorescence microscopy. *Opt. Lett.* **19**, 780–782 (1994).
19. Descloux, A., Grußmayer, K. S. & Radenovic, A. Parameter-free image resolution estimation based on decorrelation analysis. *Nat. Methods* **16**, 918–924 (2019).
20. Asokan, N. et al. Long-term in vivo imaging reveals tumor-specific dissemination and captures host tumor interaction in zebrafish xenografts. *Sci. Rep.* **10**, 13254 (2020).
21. Astell, K. R. & Sieger, D. Zebrafish in vivo models of cancer and metastasis. *Cold Spring Harb. Perspect. Med.* **10**, 1–17 (2020).
22. Sakaue-Sawano, A. et al. Visualizing spatiotemporal dynamics of multicellular cell-cycle progression. *Cell* **132**, 487–498 (2008).
23. Tebo, A. G. et al. Orthogonal fluorescent chemogenetic reporters for multicolor imaging. *Nat. Chem. Biol.* **17**, 30–38 (2021).
24. Feng, S. et al. Improved split fluorescent proteins for endogenous protein labeling. *Nat. Commun.* **8**, 370 (2017).
25. Tebo, A. G. & Gautier, A. A split fluorescent reporter with rapid and reversible complementation. *Nat. Commun.* **10**, 2822–2828 (2019).
26. Rakotoarison, L. M. et al. Improving split reporters of protein-protein interactions through orthology-based protein engineering. *ACS Chem. Biol.* **19**, 428–441 (2024).
27. Bottone, S. et al. A fluorogenic chemically induced dimerization technology for controlling, imaging and sensing protein proximity. *Nat. Methods* **20**, 1553–1562 (2023).
28. Banaszynski, L. A., Liu, C. W. & Wandless, T. J. Characterization of the FKBP-rapamycin-FRB ternary complex. *J. Am. Chem. Soc.* **127**, 4715–4721 (2005).
29. Qian, Y. et al. A genetically encoded near-infrared fluorescent calcium ion indicator. *Nat. Methods* **16**, 171–174 (2019).
30. Li, X. et al. A fluorogenic complementation tool kit for interrogating lipid droplet–organelle interaction. *J. Cell Biol.* **223**, e202311126 (2024).
31. García Casas, P. et al. Simultaneous detection of membrane contact dynamics and associated Ca2+ signals by reversible chemogenetic reporters. *Nat. Commun.* **15**, 9775 (2024).
32. Gibson, D. G. et al. Enzymatic assembly of DNA molecules up to several hundred kilobases. *Nat. Methods* **6**, 343–345 (2009).
33. Peyre, E. et al. A lateral belt of cortical LGN and NuMA guides mitotic spindle movements and planar division in neuroepithelial cells. *J. Cell Biol.* **193**, 141–154 (2011).
34. Dubois, L. et al. Amino acids bearing aromatic or heteroaromatic substituents as a new class of ligands for the lysosomal sialic acid transporter sialin. *J. Med. Chem.* **63**, 8231–8249 (2020).
35. Poirel, O. et al. LSP5-2157 a new inhibitor of vesicular glutamate transporters. *Neuropharmacology* **164**, 107902 (2020).
36. Mineev, K. S. et al. NanoFAST: structure-based design of a small fluorogen-activating protein with only 98 amino acids. *Chem. Sci.* **12**, 6719–6725 (2021).
37. Pandey, S. et al. Time-resolved serial femtosecond crystallography at the European XFEL. *Nat. Methods* **17**, 73–78 (2020).
38. Thompson, J. D., Higgins, D. G. & Gibson, T. J. CLUSTAL W: improving the sensitivity of progressive multiple sequence alignment through sequence weighting, position-specific gap penalties and weight matrix choice. *Nucleic Acids Res.* **22**, 4673–4680 (1994).
39. Wu, G., Robertson, D. H., Brooks, C. L. & Vieth, M. Detailed analysis of grid-based molecular docking: a case study of CDOCKER - a CHARMm-based MD docking algorithm. *J. Comput. Chem.* **24**, 1549–1562 (2003).

40. Krammer, A., Kirchhoff, P. D., Jiang, X., Venkatachalam, C. M. & Waldman, M. LigScore: a novel scoring function for predicting binding affinities. *J. Mol. Graph. Model.* **23**, 395–407 (2005).
41. Tinevez, J. Y. et al. TrackMate: an open and extensible platform for single-particle tracking. *Methods* **115**, 80–90 (2017).
42. Ershov, D. et al. TrackMate 7: integrating state-of-the-art segmentation algorithms into tracking pipelines. *Nat. Methods* **19**, 829–832 (2022).
43. Edelstein, A., Amodaj, N., Hoover, K., Vale, R. & Stuurman, N. Computer control of microscopes using manager. *Curr. Protoc. Mol. Biol*. https://doi.org/10.1002/0471142727.mb1420s92 (2010).

Acknowledgements

We thank K. D. Wittrup for providing us with the pCTCON2 vector and the EBY100 yeast strain for the yeast display selection. We thank V. Verkhusha for the plasmids for the mammalian expression of emiRFP670 (Addgene 136556) and miRFP713 (Addgene 136559). We thank T. Miyamoto for the plasmid for the mammalian expression of TOM20-ECFP-FRB (Addgene #171461). We thank the flow cytometry facility CISA (Cytométrie Imagerie Saint-Antoine) of UMS LUMIC at the Faculty of Medicine of Sorbonne Université, and, more particularly, Annie Munier and Angélique Vinit for their assistance. We thank the microscopy facility of the Institut de Biologie Paris Seine of Sorbonne University, and more particularly, France Lam and Chloé Chaumeton for their assistance. We thank Chloé Chaumeton from the microscopy facility of the Institut de Biologie Paris Seine of Sorbonne University, and Frédéric Eghiaian from Aberrior Instruments for their assistance for the STED imaging. This work has been supported by the European Research Council (ERC-2016-CoG-724705 FLUOSWITCH), the Agence Nationale de la Recherche (ANR-23-CE44-0014-01CATCHFIRE), the Institut Universitaire de France. LEH thanks the École Normale Supérieure and the Fondation pour la Recherche Médicale (grant FDT202304016615 to L.E.H.) for PhD funding.

Author contributions

L.E.H. and A.G. designed the overall project and wrote the paper with the help of the other authors. L.E.H., B.B., O.J., C.R., M.V., E.F., N.P., F.P., S.V., X.M., and A.G. designed the experiments. L.E.H., B.B., O.J., C.L., A.G.T., C.R., M.V., E.F., N.P., and S.V. performed the experiments. L.E.H., B.B., O.J., C.R., M.V., E.F., N.P., F.P., S.V., X.M., and A.G. analyzed the experiments.

Competing interests

The authors declare the following competing financial interests: A.G. and F.P. are co-founders and hold equity in Twinkle Bioscience/The Twinkle Factory, a company commercializing the FAST, split-FAST, and CATCH-FIRE technologies. The remaining authors declare no competing interests.

Additional information

Supplementary information The online version contains supplementary material available at https://doi.org/10.1038/s41467-025-58017-9.

Correspondence and requests for materials should be addressed to Arnaud Gautier.

Peer review information *Nature Communications* thanks Shoujun Zhu, who co-reviewed with Jia Li, and the other, anonymous, reviewer(s) for their contribution to the peer review of this work. A peer review file is available.